

Helping to reduce mining industry carbon emissions: A step-by-step guide to sizing and selection of energy efficient high pressure grinding rolls circuits

Stephen Morrell

SMC Testing Pty Ltd, Australia

ARTICLE INFO

Keywords:

Comminution
Energy efficiency
Carbon emissions
High pressure grinding rolls

ABSTRACT

Comminution is a major contributor to the Mining Industry's carbon footprint. As most of the world's leading mining companies have formally committed themselves to having net zero scope 3 carbon emissions by at least 2050, the pressure to significantly improve comminution circuit energy efficiency over the next 25–30 years will be intense. High Pressure Grinding Rolls (HPGR) circuits have the potential to reduce the Mining Industry's CO₂ emissions by up to 34.5 megatonnes/year, or 43.5% when compared to the established Autogenous (AG)/Semi-Autogenous (SAG)/Ball mill circuit alternatives. However, uptake of HPGR technology has been relatively slow. This may be due in part to the fact that costly and time-consuming pilot testing is still the norm for assessing, selecting and sizing HPGR circuits. This is in contrast to AG/SAG/Ball mill circuits where relatively cheap, fast and effective power-based methodologies are used.

To combat this limitation and help accelerate the adoption of this technology a power-based methodology has been developed which can be easily used to assess, size and select HPGR closed circuits in hard rock mining applications. Equations are derived which, on the basis of published data from manufacturers and full-scale operating plants, are demonstrated to accurately reproduce HPGR throughput capacity, installed power and specific energy for a wide range of HPGRs. A number of worked examples are included which demonstrate how the methodology can be applied in practice.

1. Introduction

All industries are facing increasing pressure to ensure that carbon emissions are reduced to help achieve the so-called 1.5 °C future. This has led to most of the major mining companies committing to significant reductions in their operational carbon footprint – in many cases by up to 30–40% in the next 10–15 years - and to place themselves in a net-zero scope 3 emissions position by 2050 (Antofagasta, 2020; AngloAmerican, 2021; Barrick Corp, 2021; BHP, 2021; Freeport-McMoran, 2020; Glencore, 2020; Newmont, 2020; Rio Tinto, 2021; Vale, 2021), and in at least one case (Fortescue, 2021) to achieve this by 2040. Comminution has been identified as a relatively large consumer of electrical energy, being responsible for up to 60–70% of a mine-sites power requirement (Daniel et al, 2010; Buckingham et al, 2011) and consequently is responsible for a significant proportion of many mining company's carbon footprints. Currently Autogenous (AG)/Semi-Autogenous (SAG)/Ball mill technology dominates comminution circuit design where grinding to relatively fine sizes is required, eg. the gold, copper, nickel, platinum, silver, lead,

zinc and low grade iron ore sectors. High Pressure Grinding Rolls (HPGR) have been found to be more energy efficient than tumbling mills such as AG/SAG and ball mills and, having been invented by the late Prof. Schönert 45 years ago, is now considered to be a relatively mature technology. However, despite its proven savings in energy and carbon emission, uptake in the technology has been relatively slow. This in part may be due to the fact that pilot testing, with all of its attendant high costs and lengthy execution time, is still seen as the principal method of obtaining data from which HPGR trade-off studies and subsequent bankable feasibility studies are based. Having a proven power-based route to cheaply, quickly and accurately assess, size and select HPGR circuits might alleviate this limitation and help accelerate adoption of this energy/carbon-saving technology.

In this paper a power-based methodology for sizing HGPR circuits closed with classifiers is described in detail and uses recently published data from a number of operational full-scale circuits to prove its validity. Much of the paper targets hard rock applications for HPGR-Ball mill circuits but the more energy efficient HPGR-HPGR alternative is also

E-mail address: steve@smccx.com.

<https://doi.org/10.1016/j.mineng.2022.107431>

Received 30 November 2021; Received in revised form 27 January 2022; Accepted 28 January 2022

Available online 21 February 2022

0892-6875/© 2022 The Author.

Published by Elsevier Ltd.

This is an open access article under the CC BY-NC-ND license

(<http://creativecommons.org/licenses/by-nc-nd/4.0/>).

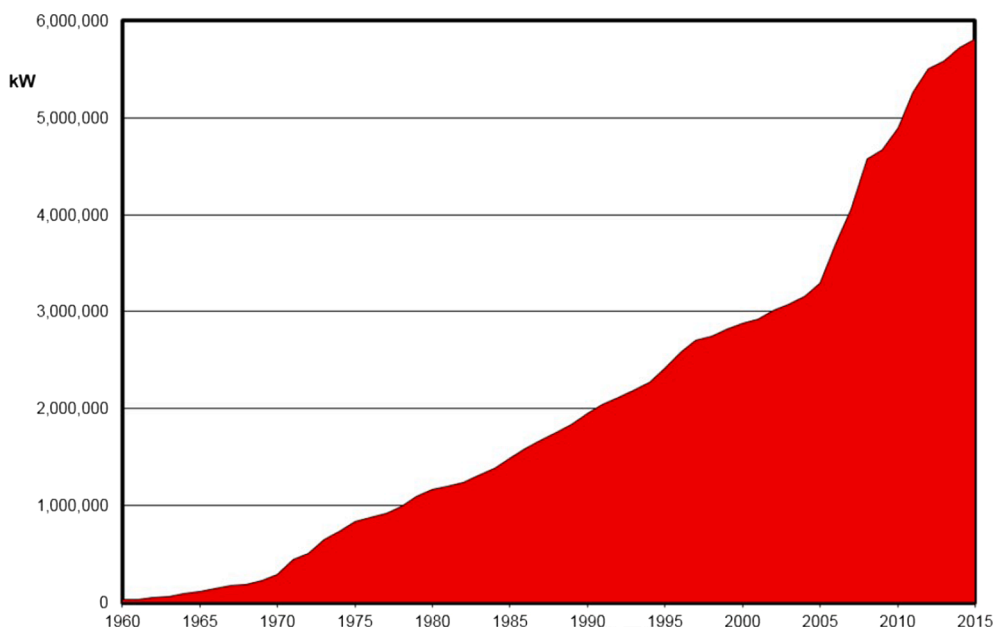


Fig. 1. Cumulative Installed Power of AG/SAG Mills (after Tozlu and Fresko, 2015).

included. Worked examples are provided in Appendixes B and C to illustrate how the methodology can be easily applied.

2. Historic perspective of AG/SAG and HPGR circuits

2.1. AG/SAG mill circuits

30 years ago AG/SAG mill circuits were still almost exclusively sized using data from pilot test programs. These were both expensive and time consuming to conduct and necessitated the use of hundreds of tonnes of sample material. This material was normally sourced via trenches that were blasted and excavated from the surface of the deposit. Not only was this also expensive it left the question unanswered as to whether the sample was representative of the entire deposit. In many cases ore deposits become harder as depth increases and caused the problem that AG/SAG circuits designed on the basis of (softer) surface samples ran the risk that after a few years when the ore became harder they would be unable to maintain target throughput. Nowadays it is rare that such pilot testing is used. Instead relatively cheap and accurate power-based techniques are used following the development of equations which accurately predict the specific energy and power draw of AG/SAG and ball mills (Morrell, 1996, 2004a, 2004b; Scinto et al., 2015; Lane et al., 2013), combined with the development of laboratory ore characterisation tests that could be carried out on small diameter drill core and that accurately reflected changes in hardness with respect to AG/SAG mill performance and location within the deposit. The development of accurate comminution simulation models and user-friendly computer programs such as JKSimMet further assisted in obviating the need for pilot test programs for AG/SAG mill circuits and helped fuel the adoption of AG/SAG technology to the point where it now dominates comminution circuit design in the Mining Industry.

2.2. HPGR circuits

The HPGR was invented by the late Prof. Schönert, who was granted a patent in 1977 (Rashidi et al., 2017). By 1984 the technology was being used in the cement industry and by the late 1980's was followed by the diamond and iron ore industries (Klymowsky, 2003; CIM Magazine, 2018). In the case of the diamond industry, HPGRs were chosen for their enhanced liberation action whilst in iron ore processing HPGRs were

used in iron ore pellet feed applications to enhance surface specific area (van der Meer, 1997, 2015) as well as for tertiary/pebble crushing (van der Meer and Maphosa, 2012; Macivor et al., 2001). In neither application was the HPGR principally chosen for its energy efficiency and almost a further 20 years had to pass before the Mining Industry saw the first full scale HPGR-Ball mill installation at Cerro Verde (Vanderbeek et al., 2006), which was chosen due to the 15% energy saving it provided compared to the SAG-Ball mill alternative. Several HPGR-Ball mill circuits have subsequently been successfully designed and installed, mainly in the copper/gold sectors such as Boddington (Hart et al., 2012), Tropicana (Kock et al., 2015), Salobo (Burns et al., 2019), Morenci (Mular et al., 2015) and Sierra Gorda (Comi and Burchardt, 2015). In all cases design of the circuit and equipment selection was based on extensive pilot testing. More recently a HPGR-HPGR dry-processing circuit has been chosen for the Iron Bridge Magnetite Project instead of the AG-ball mill alternative (Fortescue, 2019). Following an extensive on-site pilot program costing \$500 million, Fortescue reported that the results indicated energy savings of over 30% (Mining Technology, 2021). However, despite these successes uptake of this technology in the Mining Industry remains slow.

3. Carbon footprints of AG/SAG vs HPGR circuits

3.1. AG/SAG – Ball mill circuits

Tozlu and Fresko (2015) estimated that the total installed motor capacity of AG/SAG mills in hard rock mining in 2015 was 5.8 million kW (see Fig. 1). Given that mining industry activity has been relatively slow since then, additional sales of AG/SAG mill capacity from then until now (2021) would possibly be no more than 0.5 million kW. If a service life of 50 years for AG/SAG mills is assumed, then all pre-1971 sales (about 0.3 million kW) are likely to be out of use by now. Based on these assumptions it is therefore estimated that the current installed motor capacity of AG/SAG mills is about 6 million kW. Although there are a number of single stage AG/SAG mill circuits, in the vast majority of cases comminution circuits comprise AG/SAG mills followed by ball mills.

Whereas 30 years ago the rule of thumb for designing AG/SAG-Ball mill circuits was to split the total installed motor capacity 50:50 between the AG/SAG and ball mill circuits, Tozlu and Fresko's data show that in the last 20 years this has shifted considerably with the split being

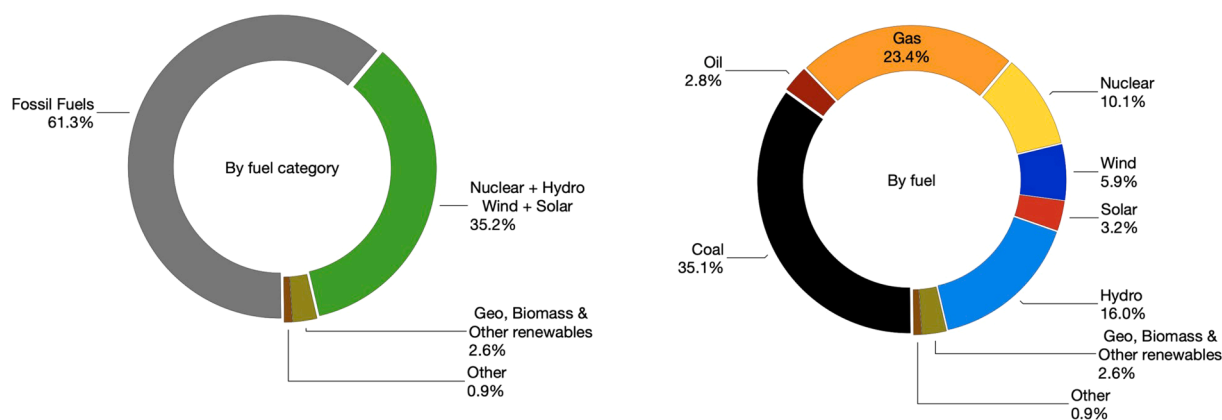


Fig. 2. Global Electricity Generation by Source for 2020 (after World Energy Data, 2021).

Table 1

Estimated Global CO₂ Emissions from AG/SAG-Ball Mill Circuits and Potential Savings Using HPGR-Ball Mill Technology.

Estimated Global Data	Units - per year	AG/SAG-Ball Mill	HPGR-Ball Mill	HPGR Circuit Savings absolute	%
Electricity consumption	TWh	116.5	99.1	17.5	15.0
CO ₂ from electricity generation	Mt	64.8	55.1	9.7	15.0
Steel ball consumption	Mt	6.5	3.7	2.9	43.9
CO ₂ from steel ball manufacture	Mt	15.0	8.4	6.6	43.9
Total CO ₂ emissions	Mt	79.8	63.5	16.3	20.4

more in favour of ball mill circuits. Using their data, it is estimated that the global installed motor capacity of AG/SAG-Ball mill circuits is split approximately 42:58 between the AG/SAG mill and ball mill circuits respectively. Thus, assuming that the global 2021 AG/SAG motor capacity is 6.0 million kW, the estimated combined AG/SAG/Ball mill installed motor capacity is of the order of 14.3 million kW. Assuming 90% utilisation of the installed power, annual operating hours of 8000, an additional 10% energy consumption for ancillaries and a 3% allowance for motor losses, equates to an estimated annual electricity consumption of 116.5 TWh (116.5 billion kWh), 48.9 TWh being consumed in the AG/SAG mill circuits and 67.6 TWh in the ball mill circuits. This compares reasonably well with Daniel et al.'s (2010) estimate of 87 TWh for comminution circuits in the mining industry, which was based on 2007 data.

3.2. Potential global carbon emission savings of HPGR circuits

Although it is perhaps unrealistic to expect that all of the existing AG/SAG-Ball mill circuits would be replaced by HPGR circuits in the near future, there have been a number of cases where HPGR's have been integrated into existing circuits with significant efficiency improvements, such as Empire, (Dowling et al, 2001), Penasquito (Palmer et al, 2011), Freeport (Villanueva et al, 2011), Cadia Hill (Engelhardt et al, 2015) and Mogalakwena (Rule et al, 2015). It is therefore worthwhile estimating what the maximum potential global impact on carbon emissions could be if HPGRs were to replace or at least be integrated with existing AG/SAG/Ball mill circuits.

3.2.1. HPGR-Ball mill circuits

If only the energy consumption of the comminution machines is considered when comparing AG/SAG-Ball mill with HPGR-Ball mill circuits then typically the latter circuits use of the order of 20–25% less

energy. However, ancillaries (conveyors, screens, transfer pumps, cyclone slurry pumps, dust extraction etc) in the HPGR-Ball mill circuit are more energy intensive and when they are taken into account the energy savings are of the order of 15% overall (Parker et al, 2001, Koski et al, 2011, Kock et al, 2015). This energy saving is via a direct reduction in the electricity consumed. As the generation of electricity results in emissions of CO₂ and other gases harmful to the environment, then by reducing electricity consumption these emissions are lessened. The extent to which this happens varies from location to location and depends on how the electricity is being generated. Coal-fired electricity generation for example produces the largest amount of carbon emissions, whilst nuclear, wind and solar produce the least. Globally the proportion of electricity generated by different methods is changing all the time, the current push being to reduce fossil-fuel use in favour of renewable sources such as wind and solar. For the purposes of calculations in this paper, the 2020 distribution of electricity generation by source has been taken from World Energy Data (2021) (see Fig. 2). Direct CO₂ emissions per kWh of electricity generated by each of these sources have been taken from the Energy Information Administration of the USA government (EIA, 2020), whilst data on lifecycle CO₂ emission of different electricity generating sources have been taken from Pehl et al. (2017). Combining these data produces an estimated global emissions rate of 0.556 kgs CO₂/kWh of electricity generated. This equates to 0.556 megatonnes/TWh (1 megatonne = 1 billion kgs; 1 TWh = 1 billion kWh). Using an estimated electricity consumption for AG/SAG-Ball mill circuits of 116.5 TWh (see Section 3.1) gives CO₂ emissions of approximately 64.8 megatonnes/year (64.8 billion kgs/year). Using an overall electrical energy saving of 15% for the HPGR-Ball mill circuit equates to a potential global saving in CO₂ emissions of 9.7 megatonnes/year (see Table 1).

Whereas it is the direct electricity consumption of comminution circuits that normally has the most attention focused on it, there are also indirect or so-called "embedded" energies that also need to be taken into consideration as they have associated CO₂ emissions. The principal source of these embedded carbon emissions is from the manufacture of steel balls which have to be regularly added to SAG and ball mills as the balls wear away (Daniel, 2007). Ball wear rates are normally represented in terms of kgs (or grams) of steel per kWh of electrical energy directly consumed by the mill. Giblett and Seidel (2011) provide steel ball wear rates from twelve of Newmont's grinding circuits from around the world and which on average give ball wear rates of 0.081 kgs/kWh and 0.049 kgs/kWh for their SAG and ball mills respectively. Assuming these figures are reasonably representative of all SAG-Ball mill circuits, then, if they are multiplied by the annual electricity consumption of SAG and ball mills the global annual consumption of steel balls can be estimated. Of course steel balls are not used in AG mills. Such mills are relatively rare and are estimated to account for no more than 3% of global motor capacity. Hence, making allowance for AG mills and

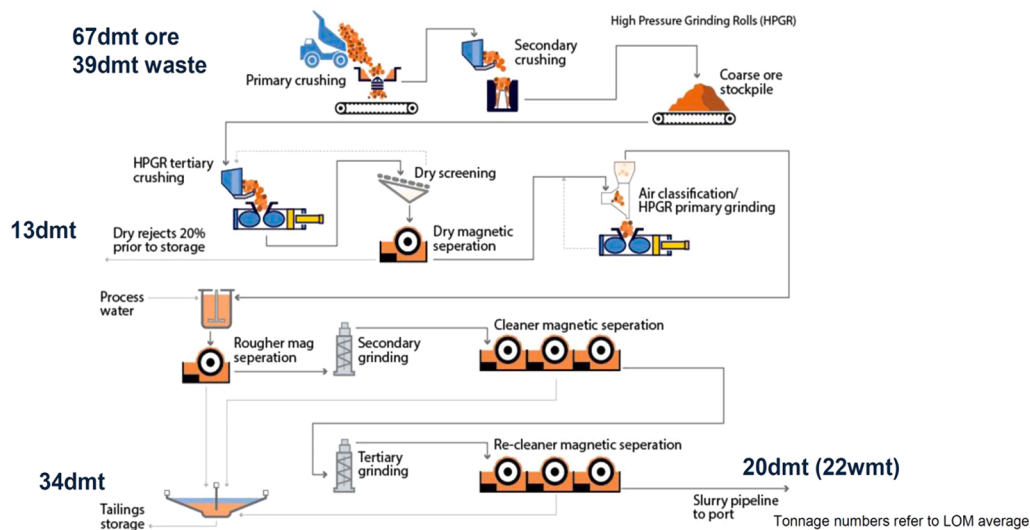


Fig. 3. Process Flowsheet for Iron Bridge Magnetite (Fortescue, 2019).

Table 2

Estimated Global CO₂ Emissions from AG/SAG-Ball Mill Circuits and Potential Savings Using HPGR-HPGR Technology.

Estimated Global Data	Units - per year	AG/SAG-Ball Mill	HPGR-HPGR	HPGR Circuit Savings absolute	%
Electricity consumption	TWh	116.5	81.6	35.0	30.0
CO ₂ from electricity generation	Mt	64.8	45.3	19.4	30.0
Steel ball consumption	Mt	6.5	0.0	6.5	100
CO ₂ from steel ball manufacture	Mt	15.0	0.0	15.0	100
Total CO ₂ emissions	Mt	79.8	45.3	34.5	43.2

omitting energy for ancillaries gives estimated direct annual electricity consumptions by SAG mills and ball mills of 43.2 TWh and 67.6 TWh respectively. On this basis the estimated annual steel ball consumptions of SAG mills and ball mills is 3.5 million tonnes and 3.0 million tonnes respectively – a total of 6.5 million tonnes/year. The World Steel Association (2017) gives a figure of 1.9 kgs of CO₂ emitted per kg of crude steel produced. Subsequent forging/casting to obtain the finished product adds, on average, a further 0.4kgs of CO₂ (Demus et al,2012; Dindorf and Wos, 2020) giving a total of 2.3 kgs CO₂ emitted per kg of steel balls consumed. This equates to a total of 14.9 megatonnes of additional CO₂ emissions per year for the AG/SAG-Ball mill circuits. Combined with the harmful gas emissions from the consumption of electricity gives a total carbon footprint of at least 79.6 megatonnes/year for AG/SAG-Ball mill circuits.

As HPGR-Ball mill circuits do not have the burden of embedded CO₂ emissions from SAG mill steel ball consumption, only the ball mill circuit needs to be considered. Ball mills in HPGR-Ball mill circuits tend to have more installed capacity than their counterparts in AG/SAG-Ball mill circuits. This is because the product size distribution from AG/SAG mills tends to have more fine material than the HPGR circuit product (Morrell, 2009, 2011) and hence need less ball mill power. Based on data from Koski et al. (2011) and Kock et al. (2015) a ball mill in a HPGR-Ball mill circuit will need about 20% more power than one in a SAG-ball mill circuit. On this basis it is estimated that the steel ball consumption of ball mills in HPGR circuits would be 3.6 million tonnes per year – a saving of 2.9 million tonnes per year compared to SAG-Ball mill circuits. This equates to a reduction in emissions of 6.6 megatonnes of CO₂ per year. Combined with the emissions saving due to the HPGR's better energy

efficiency gives a total saving of 16.3 megatonnes of CO₂ / year or 20.4% compared to AG/SAG-Ball mills (see Table 1).

3.2.2. HPGR-HPGR circuits

AG/SAG mills have similar energy efficiencies to ball mills (Morrell, 2004b). Hence, if by replacing AG/SAG mills with HPGRs energy savings of 15% are realised, then if ball mills are also replaced similar additional energy savings could be expected. This is what Fortescue Minerals found in their large scale pilot/demonstration plant at Iron Bridge (Fortescue, 2019) which is illustrated in Fig. 3. The first stage of HPGR size reduction has a similar duty to that used in HPGR-Ball mill circuits, whilst the second stage HPGR circuit replaces the relatively fine grinding that the ball mills provide. The use of HPGRs for relatively fine grinding is not new, being found in similar duties in the cement industry (Aydoğan et al., 2006) and for grinding iron ore pellet feed (van der Meer, 2015).

If the same calculation route for estimating potential global energy and CO₂ savings in Section 3.2.1 is applied to the HPGR-HPGR circuit the results shown in Table 2 are obtained. In this case it was assumed that overall energy savings amounted to 30%, as per the Iron Bridge experience. Hence potential emissions savings from improved energy efficiency amount to an estimated 19.4 megatonnes per year. Implicit in this calculation is that electricity consumption of ancillaries in HPGR-HPGR circuits is the same as in HPGR-Ball mill circuits. As the ball mill circuit is usually wet and the HPGR circuit replacing it is dry, slurry transfer pumps and cyclone feed pumps in the former will be replaced by pneumatic transfer and air classifiers in the latter. Electricity consumption for these ancillaries may well be different but at the moment there is little/no reliable published data on this subject.

As there are no SAG mills and no ball mills in the HPGR-HPGR circuit there are additional savings in CO₂ from the fact that steel ball consumption is zero. A further 15 megatonnes of CO₂ is therefore estimated to be potentially saved, giving a total saving of 34.5 megatonnes of CO₂ or 43.2% compared to a AG/SAG-Ball mill circuits.

This is a huge potential saving whose realisation might be speeded up if a relatively simple, cheap yet accurate methodology were available to assess, select and size HPGR-Ball mill and HPGR-HPGR circuits, instead of the very costly and time-consuming piloting route that is currently adopted. Such a methodology, incorporating power-based techniques, will be described in detail in the following sections.

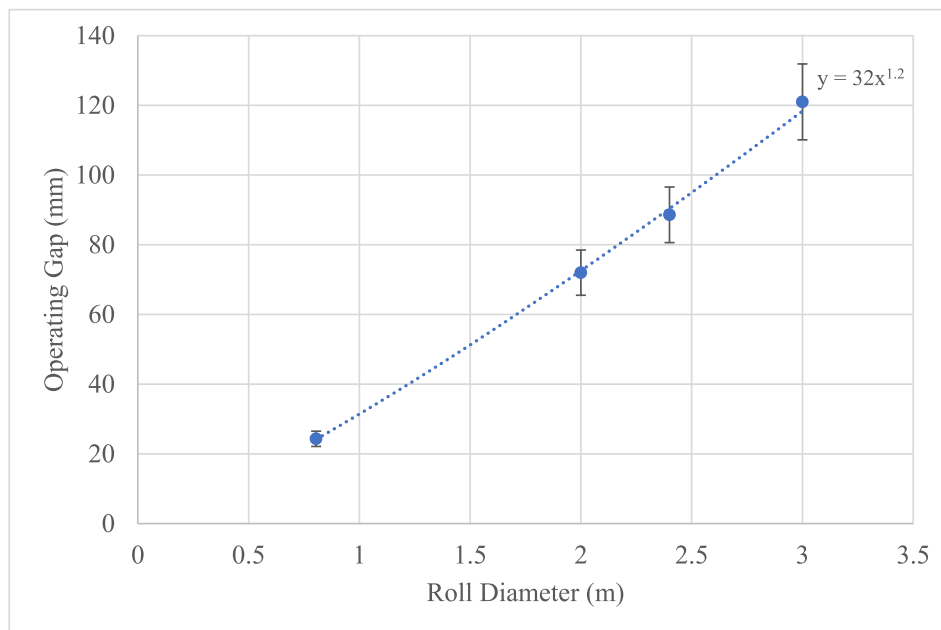


Fig. 4. Operating Gap as a Function of Roll Diameter (error bars reflect 90% CI).

4. Power-based methodology

4.1. General

The so-called power-based methodology is the current mainstay of processing engineers for helping to size and select conventional crushers, AG/SAG mills and ball mills. The methodology involves a number of steps, most of which are broadly similar regardless of the comminution circuit. However, the details in each step may differ slightly depending on the type of equipment being considered. These steps are as follows:

i. Using breakage (hardness) parameters from laboratory tests on representative ore samples, the net specific energy (kWh/t) of the machine in question is estimated. In the case of closed circuits whose classifier can be adjusted to control the product size, the equations that are used to do this will require the feed and product 80% passing size of the circuit (Bond, 1962, Morrell, 2004b, GMG Group, 2016). In the case of open circuits suitable equations usually require the 80% passing size of the feed plus a variety of data relating to the geometry of the machine and its operating settings (Sinto et al. 2015, Lane et al. 2013, Morrell, 2004a).

ii. By multiplying this net specific energy and the target throughput the required net power draw is estimated. This is often called the “design” net power draw and it is the best estimate of what the average net power draw will be when the mill is in normal use. It is usual to inflate this figure to provide a contingency which accounts for potential operational fluctuations, catch-up capacity, uncertainty and/or variability in the ore hardness data, the accuracy of the power-based equations and the risk profile of the owners of the ore deposit in question. A factor that can complicate the choice of contingency concerns the ore hardness value chosen as the basis for design. Rather than use the mean hardness value from a series of tests on representative ore samples, some engineers use, say, an 85th percentile value or a 75th percentile value etc. This value is higher than the mean and inherently provides some degree of contingency. How much of a contingency this provides is uncertain as it will depend on the spread of the of the ore hardness distribution. From a statistical viewpoint this approach is unsatisfactory, though despite this it has become quite popular. In such cases additional contingencies may be applied and will vary from project to project. If a 75th- 85th percentile hardness value is used, then an additional

contingency of the order of 5–15% may be applied. If the mean hardness is used the contingency may be up to 25%. Whatever value is used it is best decided on in collaboration with the deposit owners.

Once the contingency has been applied the resultant figure is the maximum net power that the machine will be required to deliver. The “net” for grinding mills most often relates to the power at the pinion gear shaft (or at the shell for gearless drives) and for HPGRs is usually at the roll shafts. As the purpose of this step is to determine the motor size required, further adjustments need to be made to the net power figure to allow for transmission/gearbox energy losses (usually in the range 3–7%). The resultant figure relates to the motor output power and is the required installed power.

iii. Equations (or manufacturers look-up tables) which relate the power draw to the dimensions of the machine and its operating conditions are then used to select a machine that in operation will be able to draw the required power. In choosing a suitable machine it is normal to ensure that the installed power is drawn when the equipment is operating at the extreme end of its operating envelope eg if a ball mill has been structurally designed to be operated with a maximum ball load of 40% then it should be able to draw the installed power with such a ball load. As the “design” power draw is lower than the installed power then in operation the mill will normally have a ball load lower than the maximum eg it might be 28–30%.

iv. In parallel with choosing a machine that will draw the required power it must also be ensured that the target throughput can be physically processed by the machine. This is a material transport problem and in the case of grinding mills it is usually sufficient to assume that if the machine can draw the required power it can also process the required throughput. However, some care needs to be exercised in using this assumption with closed circuit grate discharge mills, as flows may reach levels that require special attention to pulp lifter size and design (Latchireddi and Morrell, 2003). For HPGRs and conventional crushers the power draw/throughput assumption used for grinding mills is not appropriate. Hence further equations (or look-up tables) need to be applied to check that the selected machine is suitable from a throughput perspective. As with power draw, it is usual to also apply a similar contingency to the design throughput, the resultant throughput being the maximum that the machine can achieve. For example, in the case of an HPGR the maximum throughput might be matched to the machine operating at its maximum speed, the design throughput being achieved

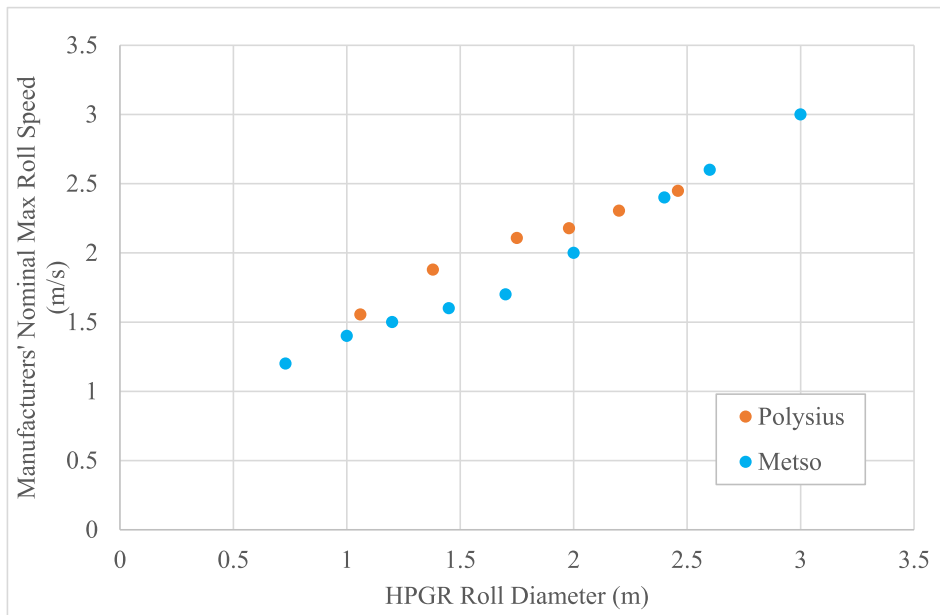


Fig. 5. Relationship Between Roll Diameter and Maximum Roll Speed as Indicated by Published Data from Polysius (2021) and Metso (2021) Equipment Catalogues.

at a lower speed.

4.2. Power-based sizing and selection of HPGRs

As the worked examples in Appendices B and C show, the general power-based methodology described in Section 4.1 requires the application of 6 key equations for HPGR circuits. The derivation of these equations is described in detail in the following sections and applies solely to HPGRs fitted with studded/textured rolls and in closed circuit with classifiers. The resultant equations do not include any effects (should they exist) due to such design characteristics as cheek plates and roll flanges nor do they include the influence of classification efficiency. This latter factor is known to affect circuit energy efficiency (Morrell, 2008) and in applying the equations described in this paper the designer must assume that the classification circuit will operate in a reasonably efficient manner.

In summary the equations relate to the following HPGR aspects:

- The relationship between roll diameter, roll length, roll speed and machine throughput capacity.
- The relationship between the specific grinding force and machine specific energy.
- The prediction of the circuit specific energy required to reduce the circuit feed F80 to the target circuit P80.
- The determination of the installed motor power.
- The estimation of the expected recycle load and the consequent throughput requirement of the machine.

4.2.1. Machine throughput capacity

Using a continuity equation and considering the passage of material as it passes between the operating gap of the HPGR, the throughput capacity can be described as follows (Klymowsky, 2003):

$$\text{Throughput } (t/h) = 3.6 \times L \times s \times u \times \rho_c \quad (1)$$

Where:

- L = Roll length (m)
- s = Mean operating gap (mm)
- u = Roll speed (m/s)

ρ_c = Cake specific gravity

Taking each term in Eq. (1) in turn, the roll length (L) is chosen from HPGR manufacturers' equipment catalogues. The mean operating gap (s) is normally reported as being a linear function of roll diameter, Klymowsky (2003) assuming that it was a linear relationship. However, combining published data from a number of pilot and full-scale operations (Parker et al, 2001; Zervas, 2019; Kock et al, 2015; Englehardt et al, 2015; Hart et al, 2011) suggests that the following power function better describes the relationship (see Fig. 4):

$$s = 32 \times D^{1.2} \quad (2)$$

where:

- s = Mean operating gap for studded/textured rolls (mm)
- D = Roll diameter (m)

It should be noted that the operating gap is principally related to the roll diameter but it is also a significant function of rolls surface. For example, a smooth roll can have up to a 40% smaller gap (all else being equal) than a studded/textured roll (Eq. (2) specifically relates to studded/textured roll surfaces). Secondary factors that can also affect the operating gap are feed size, feed size distribution, feed moisture, roll speed and operating pressure (Morley, 2010; Saramak and Kleiv, 2013).

HPGRs are often supplied with variable speed drives and two manufacturers quote the recommended speed range for each of their models in their equipment catalogues. Their nominal quoted maximum recommended speed appears to be a simple function of roll diameter; for example Fig. 5 was compiled from data published by Metso (2021) and Polysius (2021). Their data suggest the relationship between the max roll speed (u_{max}) and diameter in the range 0.7–3.0 m is:

$$u_{max}(m/s) = 0.68 \times D + 0.87 \quad (3)$$

Typically the minimum speed is of the order of 60% of u_{max} .

The cake (also known as flake) sg (ρ_c) is assumed to be 85% of the in-situ ore sg (ρ_o) (Otte, 1988; Klymowsky, 2003; Daniel, 2007). Thus:

$$\rho_c \approx 0.85 \times \rho_o \quad (4)$$

Hence an ore with an in-situ sg of 2.7 would have a cake sg of approximately 2.3. If equations 2 and 4 are substituted into Eq. (1) we

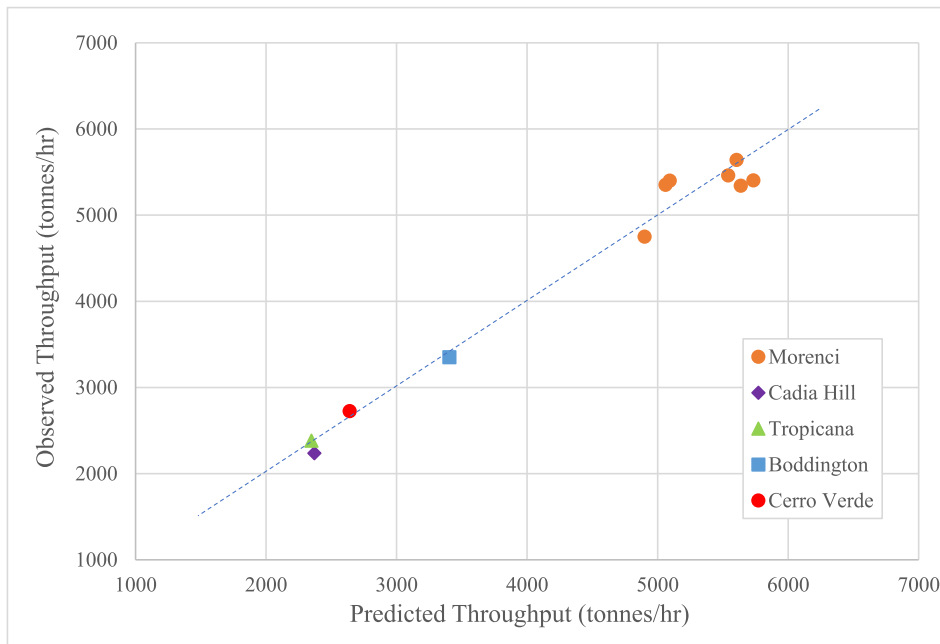


Fig. 6. Observed vs Predicted HPGR Machine Throughput.

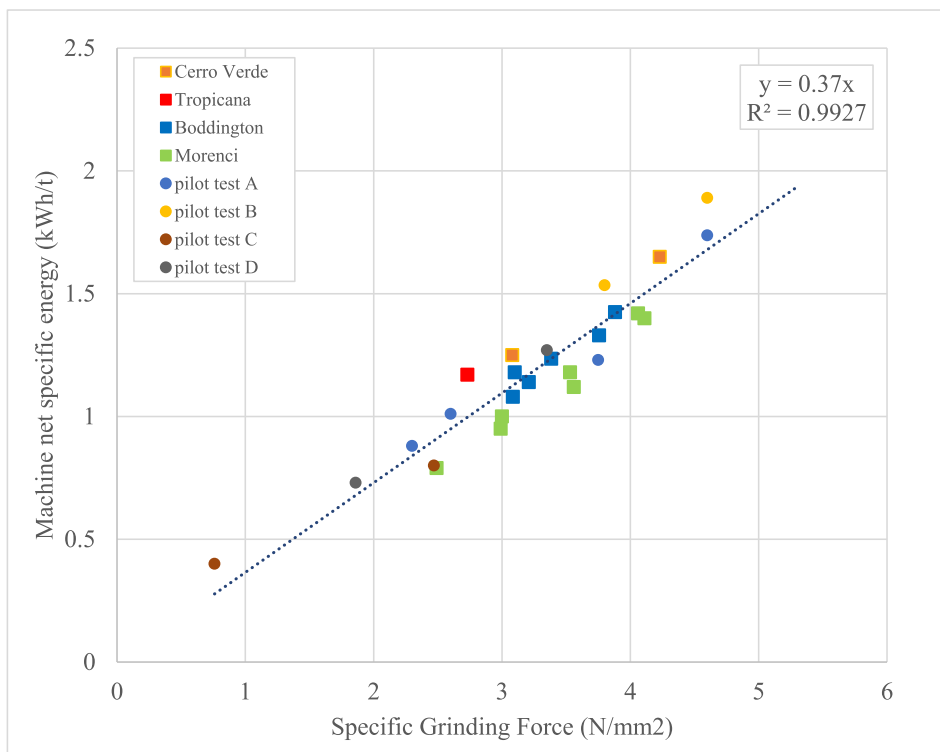


Fig. 7. Relationship Between Specific Grinding Force and Machine Specific Energy.

get:

$$Throughput(t/h) = 3.6 \times L \times 32 \times D^{1.2} \times u \times 0.85 \times \rho_o$$

$$= 98 \times L \times D^{1.2} \times u \times \rho_o \tag{5}$$

By applying Eq. (5) to the published operating data from Morenci (Zervas,2019), Boddington (Hart et al, 2011), Tropicana (Ballantyne et al, 2017), Cerro Verde (Koski et al, 2011) and Cadia Hill (Engelhardt et al., 2015) the throughput prediction results shown in Fig. 6 were

obtained. The agreement is reasonably good, with a maximum error of 6%.

Combining equations 3 and 5 gives an equation which predicts the maximum throughput for a given roll diameter, roll length and ore sg as follows:

$$Maximum\ throughput\ (t/h) = 98 \times L \times D^{1.2} \times (0.68 \times D + 0.87) \times \rho_o \tag{6}$$

This equation is useful in estimating what the ultimate throughput capacity is of a machine that is being considered for a particular duty.

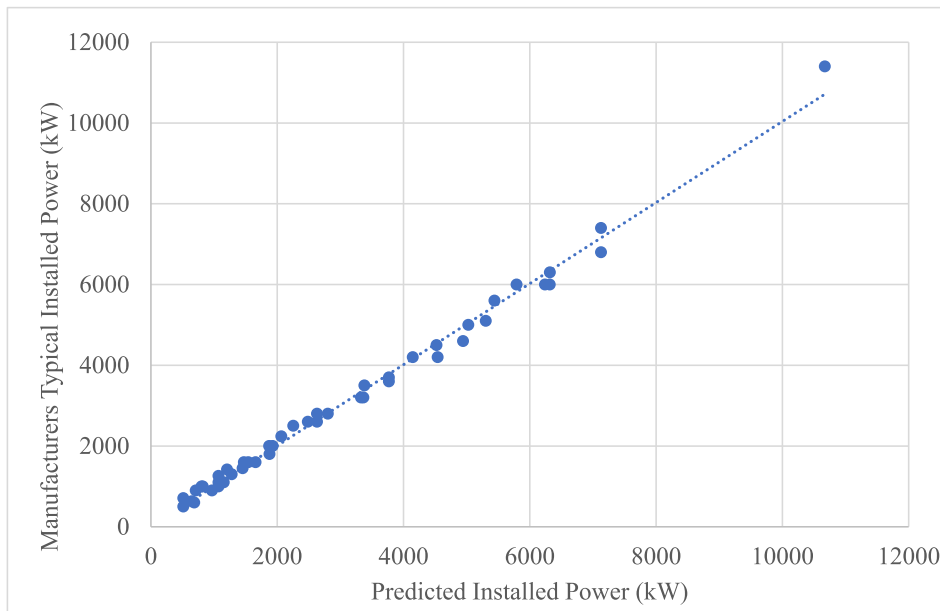


Fig. 8. Manufacturers Published Installed Power vs Predicted Using Eq. (12).

4.2.2. Specific grinding force

An HPGR principally comprises two horizontally mounted counter-rotating rolls, one being fixed, the other being free to move against a pressure applied by hydraulic pistons. Usually there are two pistons mounted on each side of the moving roll giving a total of four pistons. The pressure applied via the hydraulics can be varied which in turn varies the force applied to the feed ore via the rolls. This applied force is often quoted in terms of the specific grinding force which is defined as follows:

$$SF = \frac{F}{(1000 \times D \times L)} \quad (7)$$

Where

SF = Specific grinding force (N/mm²)
 F = Applied force (kN)
 D = Roll diameter (m)
 L = Roll length (m)

Sometimes manufacturers quote the pressure (usually in bars) applied by the hydraulic pistons rather than the applied force or specific grinding force. In such cases the specific grinding force can be determined as follows:

$$SF = \frac{(4 \times \pi \times (D_p/2)^2 \times 0.1 \times H)}{(D \times L)} \quad (8)$$

Where

D_p = Hydraulic piston diameter (m)
 H = Hydraulic pressure (bar)

Note that Eq. (8) is based on there being 4 hydraulic pistons in total. Most full-scale machines are designed to operate up to a specific grinding force of 4–5 N/mm², the maximum varying slightly from manufacturer to manufacturer. Published data indicate that most full-scale machines in the minerals industry operate in the 2–4 N/mm² range (Hart et al., 2012; Kock et al., 2015; Burns et al., 2019; Mular et al., 2015; van der Meer and Maphosa, 2013).

It has been found that the specific grinding force of the HPGR is

closely related to its net specific energy (Patzelt et al., 2000). Based on the published data from a number of full-scale installations (see Fig. 7) this relationship can be described using a simple linear function as follows:

$$W_{hm}(\text{kWh/t}) = 0.37 \times SF \quad (9)$$

Where:

W_{hm} = Machine net specific energy (machine net power draw/machine throughput, kWh/t)

The observed correlation is reasonably good, the scatter being due to secondary effects such as feed size, feed size distribution, moisture content and roll surface condition/design. The above relationship is the result of a unique feature of HPGRs in that the applied specific energy can be adjusted on line, independent of the throughput, giving them a degree of operational flexibility not found in grinding mills.

4.2.3. Installed motor power

When the HPGR is operating at maximum speed it will be running at maximum throughput capacity. If at the same time it is being operated at maximum specific grinding force it will be delivering maximum machine net specific energy. Multiplying these two maxima together will give the maximum power that the machine will be potentially able to deliver. When designing an HPGR the manufacturer therefore needs to ensure that the installed motors are large enough to provide this maximum power.

The maximum throughput capacity is described by Eq. (6), whilst the maximum net specific energy is predicted from Eq. (9) by using the maximum specific grinding force (SF_{max}) that the machine has been designed to deliver:

$$\text{Maximum machine net specific energy}(\text{kWh/t}) = 0.37 \times SF_{max} \quad (10)$$

Combining Eqs. (6) and (10), the maximum net power that the machine is capable of providing is given by:

$$\text{Maximum net power}(\text{kW}) = 36.3 \times L \times D^{1.2} \times SF_{max} \times (0.68 \times D + 0.87) \times \rho_o \quad (11)$$

The motor also has to provide power to overcome drive train losses,

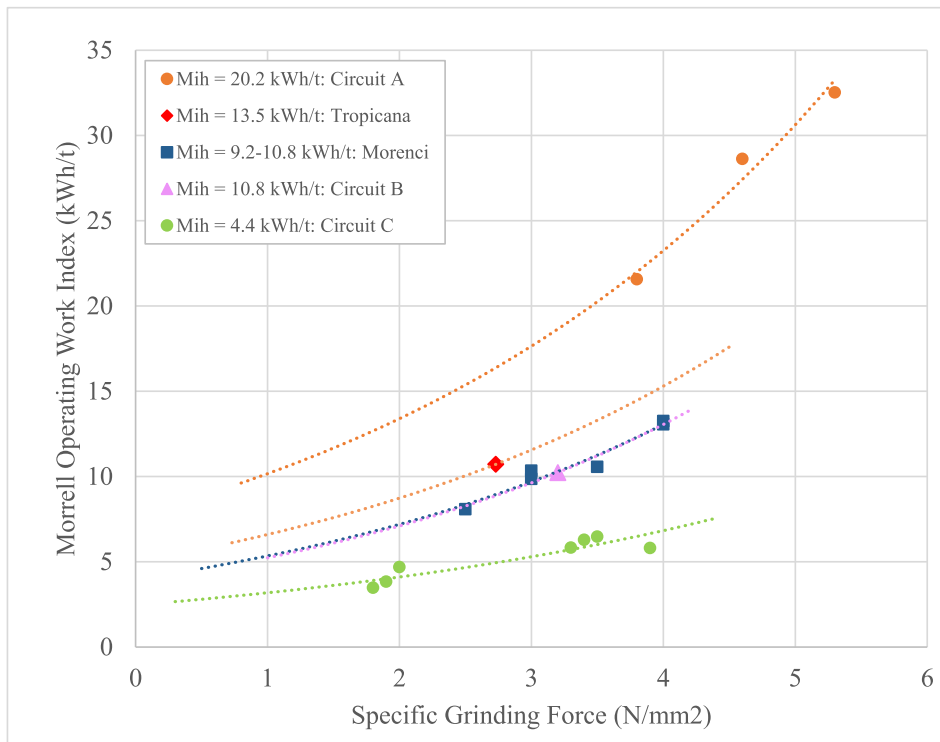


Fig. 9. Morrell Operating Work Indices vs Specific Grinding Force.

which has been assumed to be 7% of motor output power. Therefore by applying a factor of $(100/(100-7)) = 1.075$ to Eq. (11) to account for this gives:

$$\text{Installed power (kW)} = 39 \times L \times D^{1.2} \times SF_{max} \times (0.68 \times D + 0.87) \times \rho_0 \quad (12)$$

Published data on equipment specifications from HPGR manufacturers CITIC (2021), KHD (2012), Koepfer (2021), Metso (2021) and Polysius (2021) were compiled to test the above relationship. Using an in-situ ore sg (ρ_0) of 2.8, Eq. (12) was used to predict the installed power and the results compared to the manufacturers' recommended motor sizes. Fig. 8 shows the outcome, indicating a close correlation. What is significant in this correlation apart from the fact that it appears to work quite well is that it suggests that all of the HPGR manufacturers broadly agree on the relationship between design, operating conditions and resultant power draw.

4.2.4. HPGR circuit specific energy requirement

In this paper only HPGR machines in closed circuit with classifiers are considered. The specific energy of such circuits is the HPGR machine power draw divided by the circuit fresh feedrate and is the specific energy required to reduce in size the fresh feed (F_{80}) to the classifier (fine) product (P_{80}). This specific energy can be estimated using Morrell's energy-size relationship (Morrell, 2004b; GMG Group, 2016). The general form of this equation is:

$$W = M_i \times 4 \times (P_{80}^{f(P_{80})} - F_{80}^{f(F_{80})}) \quad (13)$$

Where:

W = predicted circuit net specific energy (kWh/t)

M_i = hardness parameter

$f(x) = -(0.295 + x/1000000)$

x = 80% passing size in μm

As applied to HPGR circuits the original published form of Eq. (13) is

as follows:

$$W_{hc} = M_{ih} \times S_h \times k_3 \times 4 \times (P_{80}^{f(P_{80})} - F_{80}^{f(F_{80})}) \quad (14)$$

Where:

W_{hc} = predicted net specific energy of the HPGR circuit (kWh/t)

M_{ih} = SMC Test® HPGR hardness parameter (kWh/t)

S_h = coarse feed factor

$$= 35 \times (F_{80} \times P_{80})^{-0.2} : (0.5 < S_h < 1)$$

K_3 = open/closed circuit factor

= 1.19 for open circuit

= 1.0 for closed circuit

Eq. (14) relates only to HPGRs operating with specific grinding forces in the range of 2.5–3.5 N/mm² (Morrell, 2004b). The reason for this limitation is because the size reduction energy efficiency of HPGRs is dependent on the applied specific grinding force (Klymowsky, 2003), Klymowski noting that “It is frequently more energy efficient to operate a HPGR at lower pressures....”. Hence W_h will depend on the magnitude of the specific grinding force. This was proven by Zervas (2019) in his analysis of the Morenci HPGR circuit data. He concluded that “Energy efficiency proved to decrease at greater specific forces”. This is apparent from Fig. 9 where the Morenci HPGR data plus a number of other HPGR circuits are analysed using an operating work index approach. The operating work index approach was first described by Bond (1961a) through the use of a transposed form of his energy-size equation and from which Bond operating work indices are obtained. The same methodology can be applied using Eq. (14), in which case Morrell operating work indices are obtained. The approach involves substituting the measured HPGR circuit net specific energy for W_{hc} and rearranging Eq. (14) as follows:

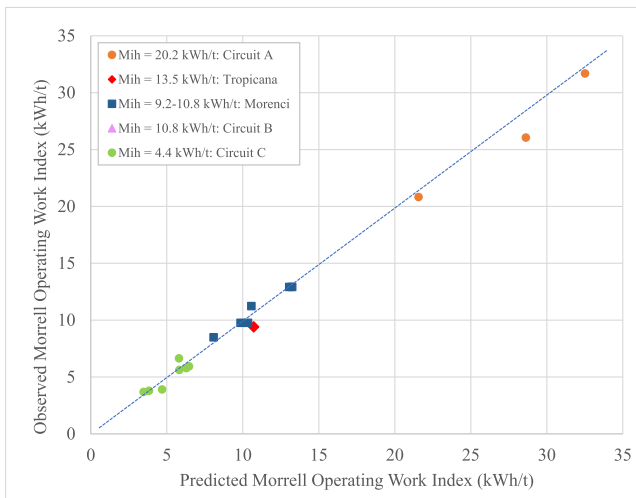


Fig. 10. Observed vs Predicted Morrell HPGR Circuit Operating Work Index.

$$M_{ih\ operating} = \frac{W_{hc\ measured}}{(S_h \times k_3 \times 4 \times (P_{80}^{f(P80)} - F_{80}^{f(F80)}))} \quad (15)$$

Where:

- $M_{ih\ operating}$ = Morrell HPGR operating work index
- $W_{hc\ measured}$ = Measured HPGR circuit net specific energy

The magnitude of the operating work index results from a combination of the inherent hardness of the feed material and size reduction energy efficiency of the HPGR circuit. For a particular hardness of feed material, the lower the Morrell operating work index the more energy efficient is the HPGR circuit. Fig. 9 shows the relationship between the Morrell operating work index and the specific grinding force of the Morenci circuit plus a number of other HPGR circuits which were chosen to represent a wide range of ore hardnesses (as indicated by the M_{ih} parameter). These results show a nest of curves, the position of each curve being related to the magnitude of the M_{ih} . Each curve has a similar

shape that indicates that the Morrell operating work index reduces as the specific grinding force reduces and hence supports Klymowski’s and Zervas’ assertions that lower specific grinding forces tend to provide more energy efficient size reduction.

Eq. (14) has no relationship to account for the influence of the specific grinding force on energy efficiency and hence in its initial development was limited to the relatively narrow range of 2.5–3.5 N/mm². Hence if it is applied to conditions outside of this range it becomes increasingly inaccurate. As Zervas (2019) noted in relation to the HPGR performance at Morenci “The (Morrell equation) prediction of circuit specific energies proved to be reasonable compared to the measured survey values, with possible exception of the higher 4.0 N/mm² scenarios” and further commented that this was consistent with published guidance (GMG, 2015) that the original Morrell equation for HPGRs was applicable only in the specific grinding force range 2.5–3.5 N/mm². To correct this limitation a new specific grinding force efficiency factor (K_4) has been developed which is based on the curves in Fig. 9. This new factor extends the applicability of Eq. (14) to the range 1.8–5.3 N/mm².

K_4 is defined as follows:

$$k_4 = \frac{(0.71 \times e^{(0.28 \times SF)})}{(M_{ih}^{0.23})} \quad (16)$$

where SF is the applied specific grinding force in N/mm².

The fit of Eq. (16) to the data in Fig. 9 is illustrated in Fig. 10.

Incorporating K_4 into Eq. (14) results in the following relationship:

$$W_{hc} = M_{ih} \times S_h \times k_3 \times k_4 \times 4 \times (P_{80}^{f(P80)} - F_{80}^{f(F80)}) \quad (17)$$

The effect of K_4 is to predict a decrease in the required specific energy to achieve a certain size reduction as the applied specific force is decreased.

4.2.4.1. Validation. Fig. 11 shows how well Eq. (17) predicts the specific energy of a range of HPGR circuits, including Morenci (Zervas, 2019) and Tropicana (Ballantyne, 2017). In relation to Morenci, Zervas (2019) used Eq. (14) in his analysis and obtained a mean relative error of 13%. The application of Eq. (17), which takes into account the influence of the specific grinding force, reduces this to <4%. The Global Mining Guidelines Group has recently adopted Eq. (17) in its 2021

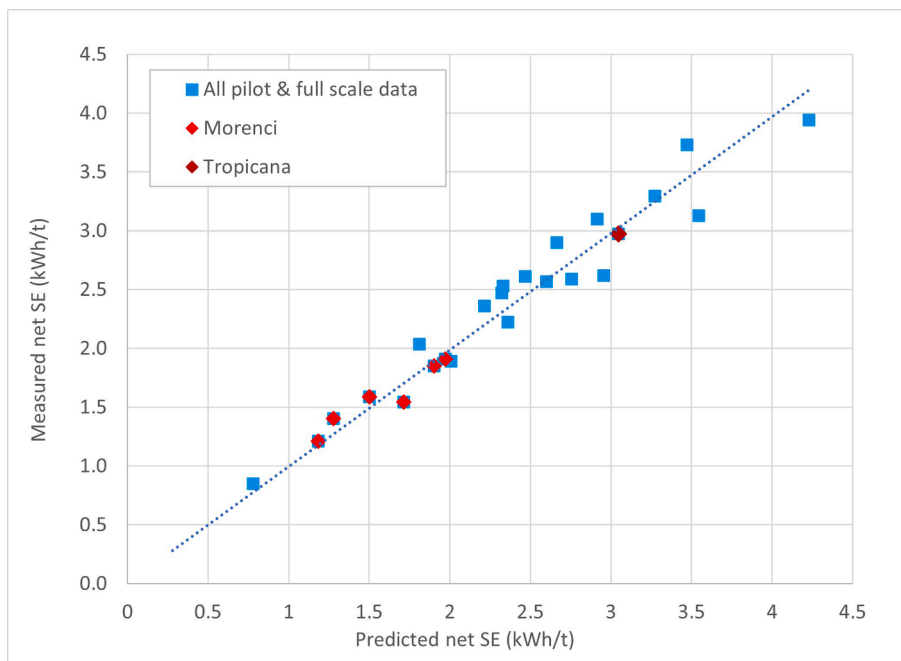


Fig. 11. Observed vs Predicted HPGR Circuit Net Specific Energy.

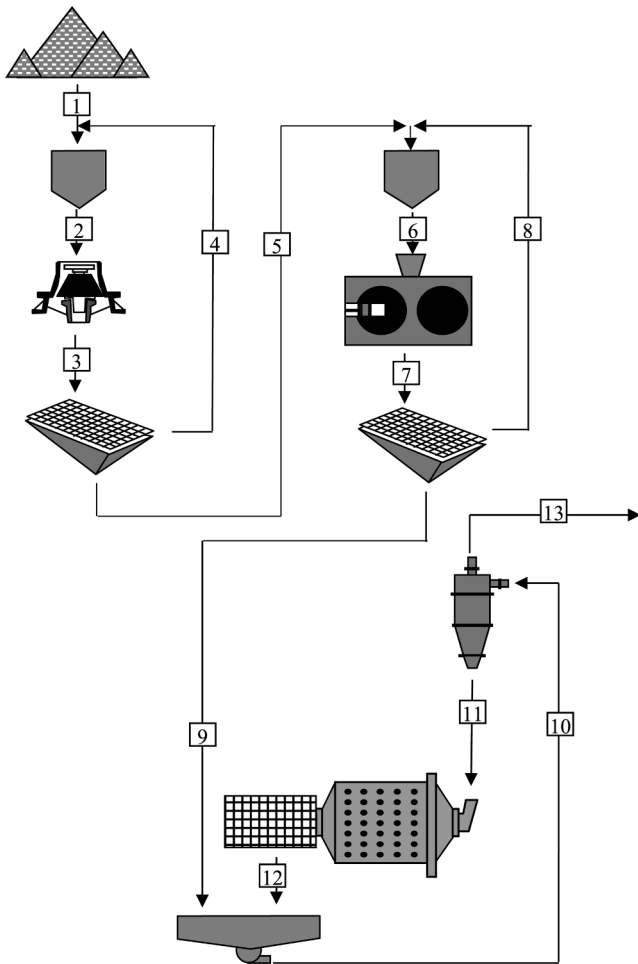


Fig. 12. Example of Crushing/HPGR/Ball Mill Circuit.

updated guidelines (GMG, 2021).

Obviously if improved size reduction energy efficiency is obtained when an HPGR is operated at a lower specific grinding force then the converse is also true. Does this mean that more and more energy is wasted as the specific grinding force is progressively increased? Stephenson (1997) clearly showed that in most cases as the applied specific grinding force increased, the Bond laboratory ball work index of the HPGR product decreased in line with the degree of microcracking that he observed under an electron microscope. Hence although the HPGR energy expenditure to achieve a given size reduction increases as the applied specific force increases, the additional energy may not be all wasted but instead might be used to save energy in the ball mill circuit

$$\text{Machine throughput requirement}(t/h) = \text{Circuit fresh feedrate} \times \left(1 + \frac{\text{recycle load}}{100}\right) \quad (26)$$

by weakening the ball mill feed. However, it is not yet clear as the specific grinding force increases whether the overall comminution circuit specific energy increases, decreases or stays the same. This subject will be considered further in the sections covering ball mill specific energy prediction (Section 4.3.1).

4.2.5. Recycle load and machine throughput requirement

Considering the HPGR circuit in the comminution flowsheet shown in Fig. 12, the recycle load is defined as:

$$\text{Recycle Load}(\%) = \frac{Tph_8}{Tph_5} \times 100 \quad (18)$$

Where:

Tph_5 = HPGR circuit fresh feedrate

Tph_8 = HPGR circuit classifier overflow (recycle) flowrate

If the HPGR machine net power draw is represented by P then the HPGR circuit net specific energy (W_{hc}) is given by:

$$W_{hc} = \frac{P}{Tph_5} \quad (19)$$

Rearranging gives:

$$Tph_5 = \frac{P}{W_{hc}} \quad (20)$$

The HPGR machine net specific energy (W_{hm}) is given by:

$$W_{hm} = \frac{P}{Tph_6} \quad (21)$$

Rearranging gives:

$$Tph_6 = \frac{P}{W_{hm}} \quad (22)$$

Also:

$$Tph_6 = Tph_8 + Tph_5 \quad (23)$$

Combining equations 20, 22 and 23 gives:

$$Tph_8 = \frac{P}{W_{hm}} - \frac{P}{W_{hc}} \quad (24)$$

Combining equations 18, 20 and 24 gives:

$$\text{Recycle Load}(\%) = \left(\frac{\frac{P}{W_{hm}} - \frac{P}{W_{hc}}}{\frac{P}{W_{hc}}} \right) \times 100$$

Hence:

$$\text{Recycle Load}(\%) = \left(\frac{W_{hc}}{W_{hm}} - 1 \right) \times 100 \quad (25)$$

As W_{hc} can be determined from Eq. (17) and W_{hm} from Eq. (9), the recycle load can be predicted using Eq. (25). In a design situation the HPGR circuit fresh feedrate (Tph_5) will be specified. By knowing the recycle load it is then possible to determine what the throughput requirement of the HPGR machine will be (Tph_6). This needs to be known so that a suitably sized machine can be chosen that is able to process material at this rate. This can be expressed as follows:

As mentioned in Section 4.2, in design situations it is usual to apply a contingency which will vary from project to project. The chosen contingency is applied to the machine throughput requirement from Eq. (26) which gives the maximum machine throughput requirement. Given a particular size of HPGR, Eq. (6) can be used to predict what the machine's maximum throughput capability is and this needs to be greater than or equal to the maximum machine throughput requirement.

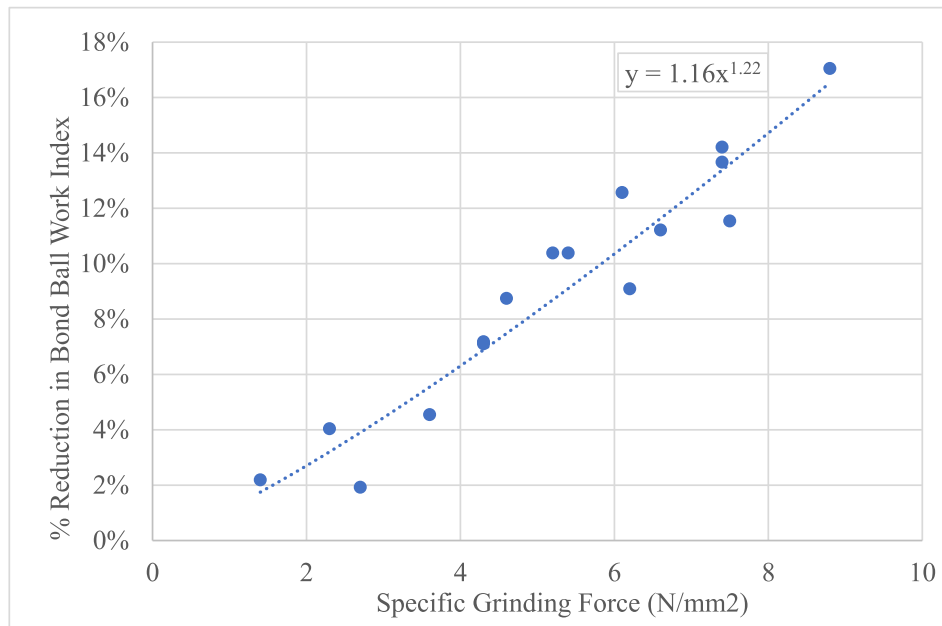


Fig. 13. Influence of HPGR Grinding Force on Bond Ball Mill Work Index Values (data after Stephenson, 1997).

4.3. Power-based sizing and selection of ball mill circuits

The methodology for sizing and selecting ball mills is somewhat simpler than with HPGRs. This is because it is usual to assume that if the ball mill has been sized correctly to draw the required power it will automatically be able to transport the required throughput. Hence additional throughput equations are not normally required. Therefore for sizing a ball mill circuit there are only three steps:

1. Predict the circuit specific energy
2. Estimate the required installed power
3. Determine the ball mill dimensions, speed and maximum ball load that will result in drawing the installed power.

4.3.1. Ball mill circuit specific energy

The ball mill circuit specific energy requirement is predicted using Eq. (13). The calculation is done in two parts. The first part takes account of the specific energy to grind relatively coarse particles (greater than 750 μm) and is represented by W_a whilst the second part takes account of grinding relatively fine particles (<750 μm) and is represented by W_b . The overall specific energy is the sum of the two. Hence to determine the specific energy to grind coarse particles (greater than 750 μm) in tumbling mills (W_a), Eq. (13) is written as:

$$W_a = M_{ia} \times 4 \times (P_{80}^{f(P80)} - F_{80}^{f(F80)}) \quad (27)$$

Where:

M_{ia} = SMC Test® coarse grinding hardness parameter

$P80 = 750 \mu\text{m}$

$$f(P80) = -(0.295 + 750/1000000)$$

$F80 = 80\%$ size of the ball mill feed (HPGR circuit product)

$$f(F80) = -(0.295 + F80/1000000)$$

For grinding finer particles (<750 μm) in tumbling mills (W_b) Eq. (13) is written as:

$$W_b = M_{ib} \times 4 \times (P_{80}^{f(P80)} - F_{80}^{f(F80)}) \quad (28)$$

Where:

M_{ib} = Hardness parameter derived using the raw data from a standard laboratory Bond ball mill work index test

$P80 =$ ball mill cyclone overflow 80% passing size in μm (ball mill circuit product size)

$$f(P80) = -(0.295 + P80/1000000)$$

$F80 = 750 \mu\text{m}$

$$f(F80) = -(0.295 + 750/1000000)$$

The sum of W_a and W_b gives the overall ball mill specific energy to which an adjustment may then be applied to account for weakening of the ball mill feed by the action of the HPGR. Research on gold ores, iron ores, bauxite, quartz and marble has shown (Stephenson, 1997) that the amount of weakening is proportional to the magnitude of the HPGR pressing force (Fig. 13). The Global Mining Guidelines Group advises that in absence of testwork on HPGR feed and product samples to determine the magnitude of this affect, an adjustment in the range 5–7% should be made (GMG Group, 2016). The relationship in Fig. 13 can also be used.

Combining equations 27 and 28 and taking into account the weakening of ball mill feed by the HPGR, the overall ball mill specific energy is given by:

$$W_{bm} = K_{hpgr} \times (W_a + W_b) \quad (29)$$

Where

W_{bm} = Overall ball mill net specific energy (kWh/t)

K_{hpgr} = Factor to account for weakening of ball mill feed by the HPGR (typically in the range 0.93–0.95)

W_a = Net specific energy to grind from ball mill feed to 750 μm

W_b = Net specific energy to grind from 750 μm to ball mill circuit product

4.3.1.1. Determination of the M_{ib} parameter. Whereas the M_{ib} parameter (Eq. (17)) and M_{ia} parameter (Eq. (27)) are obtained from a SMC Test®,

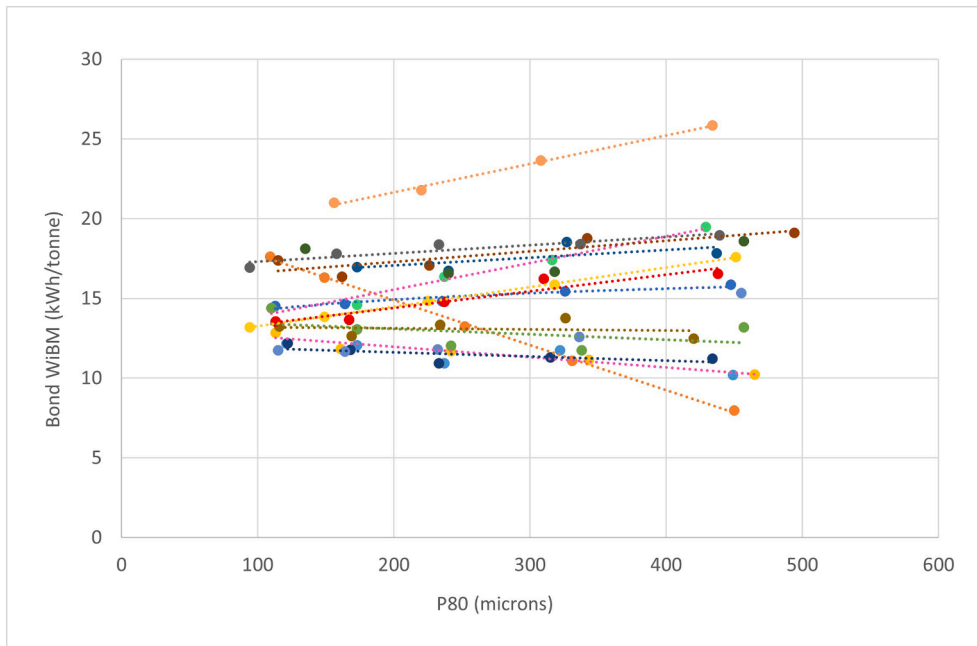


Fig. 14. Bond W_{iBM} Trends with Grind Size (Data from Bond, 1959).

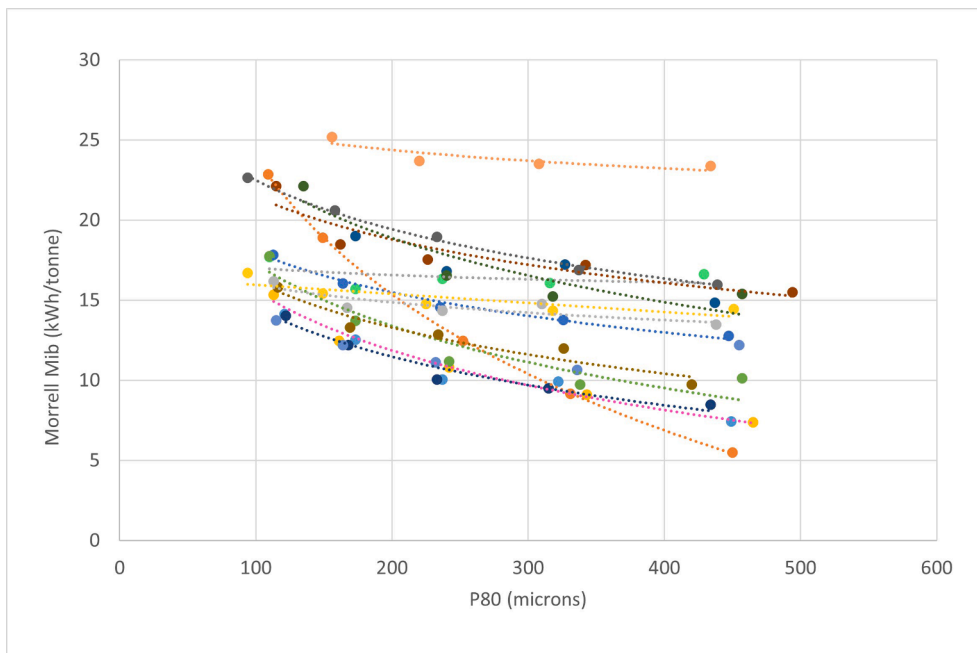


Fig. 15. Morrell M_{iB} Trends with Grind Size (Data from Bond, 1959).

the M_{iB} parameter is obtained from the raw data generated from a standard laboratory Bond ball mill work index (W_{iBM}) test (Morrell, 2008) Hence:

$$M_{iB} = \frac{18.18}{P100^{0.295} \times Gpb \times (P80^{f(P80)} - F80^{f(F80)})} \quad (30)$$

Where:

- P100 = the closing screen aperture (μm)
- Gpb = the net screen undersize product per revolution in the laboratory ball mill (g/rev)
- P80 = 80% passing size of the closing screen undersize (μm)

$F80 = 80\%$ passing size of the fresh feed (μm)

$$f(P80) = -(0.295 + P80/1000000)$$

$$f(F80) = -(0.295 + F80/1000000)$$

A worked example is given in Appendix A. If full details of the Bond laboratory work index test are not available to determine the M_{iB} , it is possible to estimate the required data if the W_{iBM} and the closing screen size or final grind are known. The details of this procedure are also described in Appendix A with associated worked examples.

Bond (1959) published the full details of laboratory ball work index tests he carried out on fifteen different ore types. For each ore type, he repeated the test at five different grind sizes to determine how the

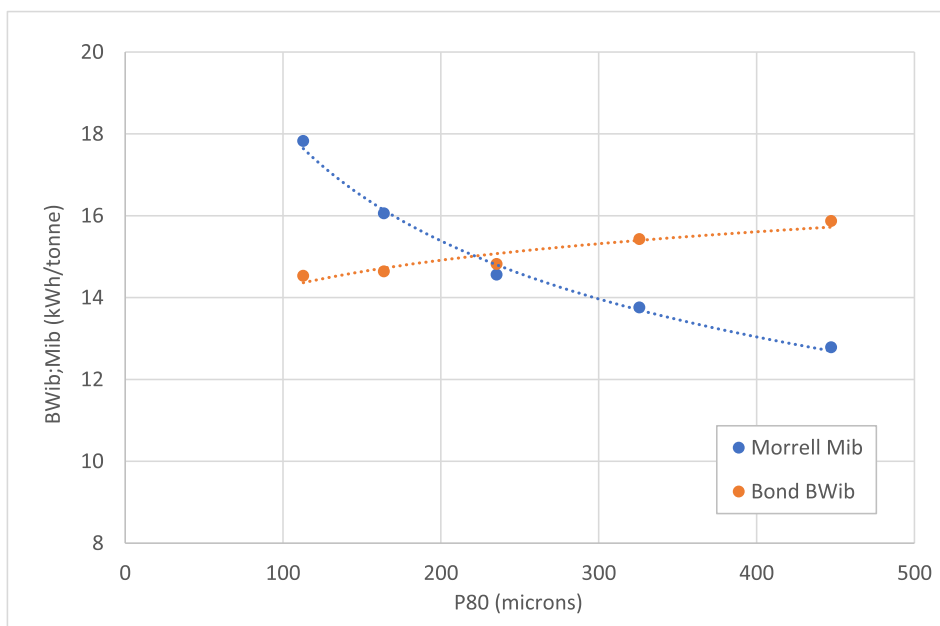


Fig. 16. Morrell M_{ib} and Bond W_{iBM} Mean Trends with Grind Size (Data from Bond, 1959).

Table 3

Cerro Verde Ore Characteristics (Data from Wong et al, 2019).

Parameter	Units	C1 BM1	C1 BM2	C1 BM3	C1 BM4	C2 BM1	C2 BM5
W_{iBM}	kWh/t	16.1	15.9	16.2	16.1	15.3	15.3
M_{ia}	kWh/t	16.8	16.8	16.8	16.8	16.8	16.8
M_{ib}	kWh/t	17.6	16.8	17.1	17.4	16.6	17.4

various test parameters and the Bond ball work index varied with grind size. Fig. 14 summarizes the resultant trends from his data and shows there is a wide spectrum of relationships, approximately half of which indicate that the Bond ball mill work index decreases with decreasing grind size ie suggesting that rocks become easier to break as they become smaller. This goes against fracture mechanics theory (Griffiths, 1921) and experimental evidence from the controlled breakage of single rock specimens (Andersen, 1988; Tavares and King, 1998; Banini, 2002). However, approximately half of Bond's results indicate the opposite, though if all his data are aggregated the results still indicate that on average the Bond ball work index tends to decrease as the grind size decreases over the range of grind sizes he tested (Fig. 16). As Bond provided all of the raw data from his testwork it is possible to calculate the associated M_{ib} values using Eq. (30). Fig. 15 shows the trends in the

M_{ib} values with respect to the grind size. In all cases, the M_{ib} increases with decreasing grind size, in line with Griffiths theory and the aforementioned experimental results on single particles. Due to the observed trends in W_{iBM} and M_{ib} with grind size both Bond (1961b) and Morrell (2008) recommended that the Bond laboratory test should be carried out at the same (or similar) grind size to the plant. It is the author's experience that this recommendation is often not adhered to, the (tacit) assumption being that the W_{iBM} and M_{ib} are material constants and are not affected by particle size.

To limit the impact of incorrect application of the M_{ib} caused by the incorrect choice of grind size in the Bond ball work index test, the relationship shown in Eq. (31) was developed. It is meant to be applied in cases where only a single Bond laboratory work index test has been done using a closing screen size that resulted in a final grind P80 which

Table 4

Cerro Verde Predicted and Measured Ball Mill Net Specific Energy (Data from Wong et al, 2019).

Source	Units	C1 BM1	C1 BM2	C1 BM3	C1 BM4	C2 BM1	C2 BM5	Mean
Bond	kWh/t	9.3	8.7	8.6	9.1	9.2	10.1	9.2
Bond-Rowland	kWh/t	8.6	8.0	8.0	8.4	8.7	9.5	8.5
Morrell	kWh/t	8.0	7.5	7.4	7.8	8.2	9.0	8.0
Measured	kWh/t	7.0	7.0	7.3	7.2	9.3	8.9	7.8

Table 5

Cerro Verde Percentage Difference Between Predicted and Measured Ball Mill Net Specific Energy (Data from Wong et al, 2019).

Source	Units	C1 BM1	C1 BM2	C1 BM3	C1 BM4	C2 BM1	C2 BM5	Mean
Bond	%	33.9	24.9	18.2	26.2	-1.0	12.8	17.8
Bond-Rowland	%	23.4	15.1	9.0	16.3	-6.4	6.5	9.6
Morrell	%	14.3	7.1	1.4	8.3	-11.8	1.1	2.6

Table 6
Tropicana Predicted and Measured Ball Mill Net Specific Energy (Data from Kock et al, 20,195 and Ballantyne et al, 2017).

Parameter	Units	Kock et al	Ballantyne et al		Average
		Plant summary	Survey 1	Survey 2	
F80	µm	2190 ¹	2190 ¹	2190 ¹	2190
P80	µm	73	103 ¹	91 ¹	89
Bond lab work index	kWh/t	16.94 ²	19.2	19.2	18.43
Morrell Mib	kWh/t	24.4	25.7	26.6	25.57
Measured ³	kWh/t	17.02	15.15	13.37	15.18
Morrell predicted	kWh/t	15.95	14.16	15.52	15.21
Difference	%	-6.29	-6.53	16.08	0.20

Notes: ¹ Interpolated from graphical plots of feed and product size distributions.
² Weighted average of primary and transition/oxide ores.
³ Reported data assumed to be based on motor input power; 6.5% motor/drivetrain losses were applied to convert to net power.

was more than 10–15% different to the P80 of interest. The exponent of 0.24 in this equation comes from fitting a power function to the M_{ib} trend in Fig. 16.

$$M_{ibtarget} = M_{ibref} \times \left(\frac{P80_{ref}}{P80_{target}} \right)^{0.24} \quad (31)$$

Where:

- $M_{ibtarget} = M_{ib}$ in the calculation that is required to be carried out
- $M_{ibref} = M_{ib}$ obtained using the data from the Bond laboratory ball work index
- $P80_{target} = P80$ of interest in the calculation that is required to be carried out
- $P80_{ref} = P80$ obtained in the Bond laboratory ball work index test

The Global Mining Guidelines Group has recently adopted Eq. (31) in its 2021 updated guidelines (GMG Group, 2021). A worked example illustrating the application of Eq. (31) can be found in Appendix A.

4.3.1.2. **Validation.** Wong et al. (2019) applied the so-called “Morrell method” as described by the GMG Group (2016) to Cerro Verde ball mill data and also compared it with Bond’s and Rowland’s methodologies. Unfortunately in the preparation of Wong et al’s paper, calculation errors in determining the M_{ib} values were made. In addition the recommended adjustment to take account of ball mill feed weakening by the HPGR was not applied. Hence the predictions of the ball mill specific energy assigned to the Morrell method were incorrect as were the conclusions concerning the accuracy of this approach. This has been acknowledged by Wong and his co-authors (Wong, 2020). The results from the correct application of the Morrell method are given in Tables 3–5. The data relate to ball mills 1–4 in the Cerro Verde C1 circuit and ball mills 1 and 5 in the C2 circuit. In conducting these calculations a K_{hpgr} factor of 0.91 to account for weakening of ball mill feed by the HPGR was applied and was determined from data reported by Cerro Verde (Koski et al, 2011). Wong et al’s calculations from applying Bond and Rowland’s methodology are also given in Tables 3–5. As can be seen, on average the Morrell method results were 2.6% higher than the measured values. Bond’s and Rowland’s methodologies on average gave 17.8% and 9.6% higher results respectively.

Further ball mill circuit data were also sourced from Ballantyne et al.

Table B1
SMC Test® Ore Hardness Parameters.

Parameter	Units	Value
sg		2.8
DW _i	kWh/m ³	6.8
M _{ia}	kWh/t	19.4
M _{ic}	kWh/t	7.2
M _{ih}	kWh/t	13.9

Table B2
Bond Ball Work Index Test Results.

Parameter	Units	Value
Gpb	gms/rev	1.42
P100	µm	150
P80	µm	114
F80	µm	2325

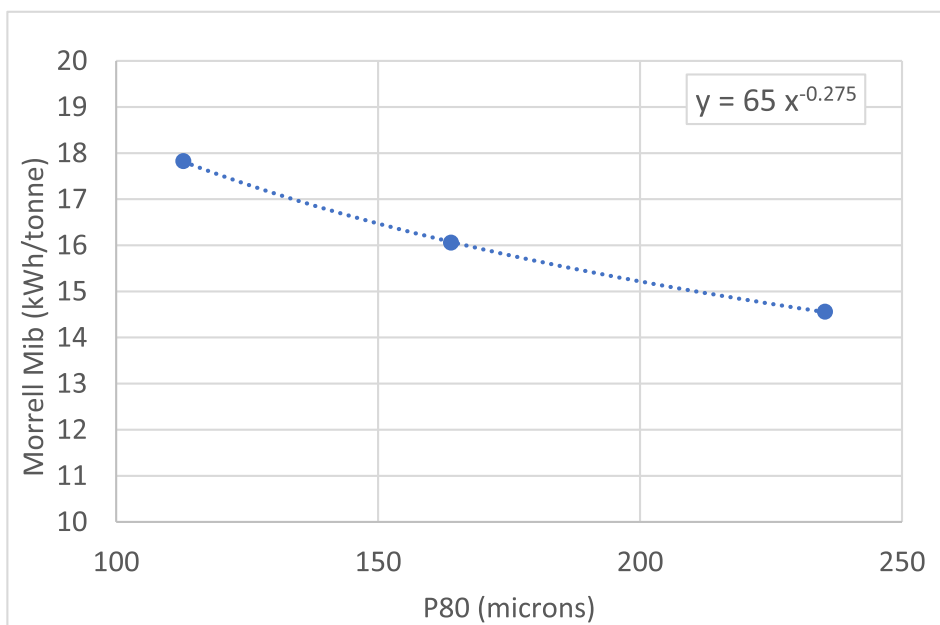


Fig. A1. Example of Trend in M_{ib} with P80.

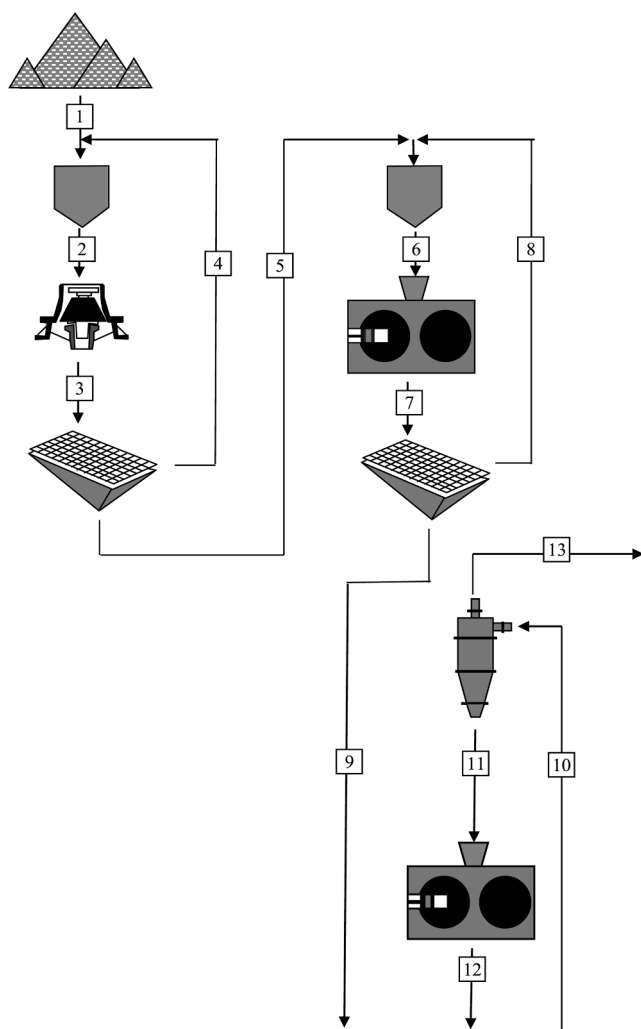


Fig. C1. Example of Crushing/HPGR/HPGR Circuit.

Table B3
SMC Test Ore Hardness Parameters.

Parameter	Units	Value
sg		2.8
DW_i	kWh/m ³	6.8
M_{ia}	kWh/t	19.4
M_{ic}	kWh/t	7.2
M_{ih}	kWh/t	13.9

(2017) from work they did on the HPGR/Ball mill circuit at Tropicana as well as Kock et al. (2015). Their results are presented in Table 6 together with predictions using Morrell's approach. A K_{hpgr} factor of 0.96 was applied to account for weakening of ball mill feed by the HPGR. This was based on the relationship in Fig. 13 and the typical Tropicana HPGR operating specific grinding force of 2.7 N/mm² that was reported by Kock et al. (2015). On average the predictions were 0.2% higher than the measured values. The data in Table 6 are interesting in that the measured values suggest that even though the grind size in survey 2 was finer than survey 1, less energy was used in survey 2 it appeared that the circuit was more energy efficient. Ballantyne et al. suggested that this was due to the fact that the ball mill circuit in survey 2 was more energy efficient. In survey 2 the ball mill speed was reduced from 83% of critical to 76% and it was hypothesized that this might have resulted in a trajectory change which created more favourable breakage conditions. Whether this was the case remains to be seen as Ballantyne et al. also

hypothesized that as the ball mill had a Slip Energy Recovery (SER) motor it could also be possible that the apparent change in grinding efficiency was in fact caused by changes in the SER efficiency with speed.

4.3.2. Installed motor power

Having estimated the required ball mill circuit net specific energy, it is then required to estimate the installed power. The initial step is to multiply the required ball mill circuit net specific energy by the target throughput. The resultant power draw is the best estimate of what the average net power draw will be when the ball mill circuit is running under normal, steady state operating conditions. It is usual to apply a contingency that accounts for potential operational fluctuations, catch-up capacity, uncertainty and/or variability in the ore hardness data and the risk profile of the owners of the ore deposit in question. Its magnitude therefore varies from project to project. As mentioned in Section 4.1 it also depends on the hardness value on which the design is to be based e.g. a mean value or a 75th percentile, 85th percentile etc. If the mean hardness is selected on which to base the design then a typical contingency is about 25%. At this point the resultant power draw will be in net terms. For grinding mills this usually relates to the power at the pinion gear shaft for a gear-and-pinion drive or at the shell for a gearless (wrap-around) drive. As the purpose of this step is to determine the motor size required, where motor size relates to its output power capacity, adjustments have to be made to the net power figure to allow for transmission/gearbox energy losses (usually of the order of 3–4%). The resultant figure will then relate to the motor output power capacity – usually referred to as the installed power.

4.3.3. Ball mill dimensions and operating conditions

The final step is to choose a ball mill diameter, length and speed that will draw the installed power when loaded with the mill's maximum allowable ball load. The maximum ball load needs to be chosen in conjunction with the equipment supplier as it is related to the structural integrity of the mill shell, which in turn is related to such factors as the shell thickness, steel composition, design and dimensions. To predict power draw based on mill dimensions etc. a power model such as Morrell's "C" model (Morrell, 1996) is used. The equations of this model can be easily entered into a spreadsheet or alternatively can be accessed on-line via the link <https://www.smctesting.com/tools/gross-power>. This model predicts the motor input (gross) power of ball mills with a high degree of accuracy (Morrell, 2003). As motor size is based on motor output power the gross power needs to be adjusted to account for motor energy losses (usually of the order of 3%).

5. Conclusions

HPGR-Ball mill circuits have the potential to reduce the Mining Industry's CO₂ emissions by 16.3 megatonnes/year when compared to AG/SAG/Ball mill circuits. This saving climbs to 34.5 megatonnes/year if HPGRs are also used instead of ball mills. Despite this huge potential saving, uptake of HPGR technology has been relatively slow. This may be due in part to the fact that costly and time consuming pilot testing is still the norm for assessing, selecting and sizing HPGR-Ball mill circuits. This is in contrast to AG/SAG/Ball mill circuits which are normally assessed, selected and sized using the relatively cheap and effective power-based methodology.

Equations have been derived which, on the basis of published data from manufacturers and full-scale operating plants, accurately reproduce HPGR throughput capacity, installed power and specific energy for a wide range of HPGRs in the hard rock mining sector. This includes the largest machines currently in operation.

Analysis of published data on the influence the specific grinding force has confirmed assertions by a number of engineers and researchers that higher specific grinding forces result in a drop in comminution efficiency. Hence, the HPGR has to use additional energy to achieve a similar size reduction than when operating at lower specific grinding

forces. As further published research has indicated that higher specific grinding forces result in weakening of the HPGR products, the additional energy may not be necessarily wasted but may save some energy in the downstream ball mill circuit. How this affects the overall energy consumption comminution circuits is not clear at this stage.

In recognition of the influence of specific grinding force on HPGR efficiency, an additional term has been added to the so-called “Morrell method” for predicting HPGR circuit specific energy. This extends the applicable range of this method to 1.8–5.3 N/mm². This has been adopted by the Global Mining Guidelines Group.

Using a new equation that accounts for the influence of specific grinding force on HPGR energy efficiency the “Morrell method” is shown to predict closed circuit HPGR performance to within 6.5% on average.

Analysis of published data on the performance of ball mills that follow HPGR circuits indicates that the “Morrell method” predicts ball mill circuit performance to within 3% on average. This analysis includes allowances for weakening of the HPGR product due to microcracking of ore particles and hence suggests that this phenomenon is observed in full-scale operating comminution circuits.

Appendix A. Determination of M_{ib} : Worked examples

A.1. Determination of the M_{ib} where full details of the laboratory Bond ball mill work index test are available

The M_{ib} equation is given below and uses the following inputs from the standard laboratory Bond ball mill work index test (Bond, 1961a):

- M_{ib} = hardness parameter for grinding particles < 750 μm (kWh/t)
- G_{pb} = net screen undersize product per revolution of the last cycle (g/rev)
- P_{100} = closing screen size (μm)
- P_{80} = 80% passing size of the closing screen undersize of the last cycle (μm)
- F_{80} = 80% passing size of the new feed (μm)

$$M_{ib} = \frac{18.18}{P_{100}^{0.295} \times G_{pb} \times (P_{80}^{-(0.295+P_{80}/1000000)} - F_{80}^{-(0.295+F_{80}/1000000)})} \quad (\text{A1})$$

The value of the M_{ib} is valid for the P_{80} obtained in the associated Bond ball mill work index (W_{iBM}) test and if the choice of closing screen size has been made correctly should be similar to the P_{80} of interest in the circuit being designed/studied ($P_{80_{\text{target}}}$). If calculations are required to be carried out using P_{80} values significantly different to that obtained in the laboratory test (greater than 10–15%) then ideally further W_{iBM} tests should be carried out using more appropriate closing screen sizes. Where it is known in advance that a series of calculations will be carried out using a range of P_{80} values, the best approach is to do at least two W_{iBM} tests (preferably 3) in which the closing screen sizes are chosen so that the resultant P_{80} s achieved in the tests bracket the P_{80} range of interest. As a general guide the P_{80} achieved in the W_{iBM} test is usually about 0.76 of the closing screen size and hence this approximation can be used to guide the choice of suitable closing screen sizes. Having carried out the appropriate W_{iBM} tests and applied equation A1 to the raw data, the resulting M_{ib} values can then be plotted as per the example in Fig. A1. Depending on the P_{80} being targeted the required M_{ib} value can be either read off the plot or estimated using a fitted equation such as the one shown in the figure.

In situations where only one W_{iBM} test has been done and trends such as that shown in Fig. A1 are not available, then if it is required to carry out calculations using a target P_{80} which is more than 10–15% different to the one achieved in the laboratory test, Eq. (A2) can be used.

$$M_{ib_{\text{target}}} = M_{ib_{\text{ref}}} \times \left(\frac{P_{80_{\text{ref}}}}{P_{80_{\text{target}}}} \right)^{0.24} \quad (\text{A2})$$

Where:

- $M_{ib_{\text{target}}}$ = M_{ib} in the calculation that is required to be carried out
- $M_{ib_{\text{ref}}}$ = M_{ib} obtained using the data from the Bond laboratory ball work index
- $P_{80_{\text{target}}}$ = P_{80} of interest in the calculation that is required to be carried out
- $P_{80_{\text{ref}}}$ = P_{80} obtained in the Bond laboratory ball work index test

A.1.1. Worked example

A Bond laboratory ball mill work index test was conducted and generated the following results:

- P_{100} = 150 μm
- P_{80} = 109 μm
- F_{80} = 2124 μm

The results of this work suggest that power-based techniques, embodied in the “Morrell method”, are able to accurately predict HPGR/ball mill circuit performance and hence are a reliable approach for assessing, sizing and selecting suitable HPGRs and ball mills in green field design scenarios.

Declaration of Competing Interest

The authors declare that they have no known competing financial interests or personal relationships that could have appeared to influence the work reported in this paper.

Acknowledgments

I would like to acknowledge the owners of the Cerro Verde, Empire, Freeport, Mogalakwena, Tropicana, Morenci, Cadia Hill, Sierra Gorda and Boddington mines for allowing various papers to be published which contain data on the performance of their HPGR/ball mill circuits. Without such data being made readily available our industry will not move forward.

Using the above inputs M_{ib} is calculated using Eq. (A1) as follows:

$$M_{ib} = \frac{18.18}{150^{0.295} \times 1.75 \times \left(109^{-(0.295+109/1000000)} - 2124^{-(0.295+2124/1000000)}\right)}$$

Hence:

$$M_{ib} = 16.0 \text{ kWh/t}$$

This is valid for P80s of the order of 109 μm . The ball mill specific energy for a P80 of 75 μm is required to be calculated. So the M_{ib} for a P80 of 75 μm needs to be determined as follows:

Input Data:

M_{ib} calculated from the Bond test (M_{ibref}) = 16.0 kWh/t

Reference P80 from the Bond test ($P80_{ref}$) = 109 μm

Target P80 ($P80_{target}$) = 75 μm

Calculations:

From Eq. (A2):

$$M_{ibtarget} = 16.0 \times \left(\frac{109}{75}\right)^{0.24}$$

Hence:

$$M_{ib} = 17.5 \text{ kWh/t}$$

A.2. Determining the M_{ib} where full details of the Bond ball mill laboratory test are not available

In some situations W_{iBM} values may be available but not the Gpb, P100, P80 and F80 details of the test which are necessary to generate the M_{ib} values. In such circumstances certain assumptions may be made which enable the M_{ib} values to be estimated. Two situations will be considered. The first is where the W_{iBM} value is known as well as the closing screen size used (P100). The second case is where the W_{iBM} value is known but nothing else. In both of these cases Bond's equation for calculating the W_{iBM} from laboratory test data is used. This equation is as follows:

$$W_{iBM} = \frac{49.05}{P100^{0.23} \times (Gpb)^{0.82} \times 10 \times \left(\frac{1}{\sqrt{P80}} - \frac{1}{\sqrt{F80}}\right)} \quad (A3)$$

This equation can be rearranged as follows:

$$Gpb = \left\{ \frac{4.905}{P100^{0.23} \times W_{iBM} \times \left(\frac{1}{\sqrt{P80}} - \frac{1}{\sqrt{F80}}\right)} \right\}^{\left(\frac{1}{0.82}\right)} \quad (A4)$$

A.2.1. W_{iBM} value and closing screen size (P100) are known

With reference to equation A4, the only unknowns in this situation are the P80 and F80. As a general rule the P80 is typically 0.76 of the P100 and on average the F80 is about 2250 μm . Using these assumptions in equation A4, Gpb can be estimated as follows:

$$Gpb_{est} = \left\{ \frac{4.905}{P100^{0.23} \times W_{iBM} \times \left(\frac{1}{\sqrt{0.76 \times P100}} - \frac{1}{\sqrt{2250}}\right)} \right\}^{\left(\frac{1}{0.82}\right)} \quad (A5)$$

We now have estimates of the Gpb, P80 and F80 and we know P100. Hence we can use these values in equation A1 to estimate M_{ib} :

$$M_{ib} = \frac{18.18}{P100^{0.295} \times Gpb_{est} \times \left((0.76 \times P100)^{-\left(0.295 + \left(\frac{0.76 \times P100}{1000000}\right)\right)} - 2250^{-\left(0.295 + \frac{2250}{1000000}\right)} \right)} \quad (A6)$$

A.2.1.1. Worked example. A laboratory Bond ball work index test has been carried out using a closing screen size of 150 μm and it returned a W_{iBM} value of 13.2 kWh/t.

Using Eq. (A5):

$$G_{pb_{est}} = \left\{ \frac{4.905}{P150^{0.23} \times 13.2 \times \left(\frac{1}{\sqrt{0.76 \times 150}} - \frac{1}{\sqrt{2250}} \right)} \right\}^{\left(\frac{1}{0.82} \right)}$$

$$= 1.80 \text{ g/rev}$$

Using Eq. (A6):

$$M_{ib} = \frac{18.18}{150^{0.295} \times 1.80 \times \left((114)^{-\left(0.295 + \frac{114}{1000000}\right)} - 2250^{-\left(0.295 + \frac{2250}{1000000}\right)} \right)}$$

Hence:

$$M_{ib} = 15.8 \text{ kWh/t}$$

A.2.2. Only $W_{i_{BM}}$ value is known

With reference to Eq. (A4), in this situation the unknowns are the Gpb, P100, P80 and F80. In this case the assumption is made that the $W_{i_{BM}}$ test has been carried out with a closing screen size that produced a P80 which is the same as the target P80 ($P80_{target}$). As the P80 is typically 0.76 of the P100, if we know the P80 then P100 can be estimated as follows:

$$P100_{est} = \frac{P80_{target}}{0.76} \quad (A7)$$

If the assumption that F80 is 2250 μm is made then Gpb can be estimated using equation A5 as follows:

$$G_{pb_{est}} = \left\{ \frac{4.905}{P100_{est}^{0.23} \times W_{i_{BM}} \times \left(\frac{1}{\sqrt{P80_{target}}} - \frac{1}{\sqrt{2250}} \right)} \right\}^{\left(\frac{1}{0.82} \right)} \quad (A8)$$

M_{ib} can now be estimated using Eq. (A1) as follows:

$$M_{ib} = \frac{18.18}{P100_{est}^{0.295} \times G_{pb_{est}} \times \left((P80_{target})^{-\left(0.295 + \left(\frac{P80_{target}}{1000000}\right)\right)} - 2,250^{-\left(0.295 + \frac{2250}{1000000}\right)} \right)} \quad (A9)$$

A.2.2.1. Worked example. A laboratory Bond ball work index test has been carried out and it returned a $W_{i_{BM}}$ value of 13.2 kWh/t. Calculations need to be done involving a target grind P80 of 106 μm . It is assumed that the $W_{i_{BM}}$ is the correct value for a 106 μm grind. Using equation A7 the estimated P100 is therefore given by:

$$P100_{est} = \frac{106}{0.76}$$

$$= 139.5 \text{ } \mu\text{m}$$

If the assumption that F80 is 2250 μm is made then Gpb can be estimated using equation A5 as follows:

$$G_{pb_{est}} = \left\{ \frac{4.905}{139.5^{0.23} \times 13.2 \times \left(\frac{1}{\sqrt{106}} - \frac{1}{\sqrt{2250}} \right)} \right\}^{\left(\frac{1}{0.82} \right)}$$

$$= 1.73 \text{ g/rev}$$

M_{ib} can now be estimated using equation A1 as follows:

$$M_{ib} = \frac{18.18}{139.5^{0.295} \times 1.73 \times \left((106)^{-\left(0.295 + \left(\frac{106}{1000000}\right)\right)} - 2250^{-\left(0.295 + \frac{2250}{1000000}\right)} \right)}$$

$$= 16.1 \text{ kWh/t}$$

Appendix B. Sizing and selecting a HPGR-Ball mill circuit: Worked example

In this worked example the flowsheet option shown in Fig. 12 has been chosen as the preferred comminution circuit. The secondary crushing

circuit, which feeds the HPGR circuit has already been designed and equipment selected to deliver crushed feed to the HPGR circuit with an 80% passing size of 30 mm. The requirement of the HPGR circuit is to reduce this feed to an 80% passing size of 2.2 mm by operating the HPGR in closed circuit with a vibrating screen. The target circuit throughput rate is 1000 tph. This material is then to be fed to a ball mill in closed circuit with hydrocyclones with a target overflow P80 of 150 μm (see Table B1 and B2).

SMC Tests and Bond ball mill work index tests have been carried out on representative ore samples and the following results, which are the best estimates of the mean hardness values of the deposit, have been chosen as the basis for design:

Step 1 - Using the above inputs M_{ib} is calculated using equation A1 as follows:

$$M_{ib} = \frac{18.18}{150^{0.295} \times 1.42 \times (114^{-(0.295+114/1000000)} - 2325^{-(0.295+2325/1000000)})} \quad (A1)$$

$$= 19.8 \text{ kWh/t}$$

This is valid for P80s of the order of 114 μm so the next step is to determine what the M_{ib} value is for a target P80 of 150 μm .

Step 2 – Determination of M_{ib} value for a target P80 of 150 μm :

Input Data:

M_{ib} calculated from the Bond test (M_{ibref}) = 19.8 kWh/t

Reference P80 from the Bond test ($P80_{ref}$) = 114 μm

Target P80 ($P80_{target}$) = 150 μm

Calculations:

From Eq. (A2):

$$M_{ibtarget} = 19.8 \times \left(\frac{114}{150}\right)^{0.24} \quad (A2)$$

$$= 18.5 \text{ kWh/t}$$

Step 3 - Choose an HPGR operating specific grinding force and determine the machine specific energy:

Most full-scale circuits operate in the specific grinding force (SF) range 2–4 N/mm^2 so choose 3 N/mm^2 . Using Eq. (9):

$$W_{hm} (\text{kWh/t}) = 0.37 \times SF \quad (9)$$

Hence:

$$W_{hm} = 0.37 \times 3$$

$$= 1.11 \text{ kWh/t}$$

Step 4 - Predict the HPGR circuit specific energy (W_{hc}) to reduce the circuit feed with an F_{80} of 30000 μm to a circuit product with a P_{80} of 2200 μm .

This is done using Eq. (17):

$$W_{hc} = M_{ih} \times S_h \times k_3 \times k_4 \times 4 \times (P_{80}^{f(P80)} - F_{80}^{f(F80)}) \quad (17)$$

Where:

W_{hc} = predicted net specific energy of the HPGR circuit (kWh/t)

M_{ih} = SMC Test® HPGR hardness parameter (kWh/t)

= 13.9 kWh/t

S_h = coarse feed factor

= $35 \times (F_{80} \times P_{80})^{-0.2} : (0.5 < S_h < 1)$

= $35 \times (30000 \times 2200)^{-0.2}$

= 0.955

K_3 = open/closed circuit factor

= 1.0 for closed circuit

$$k_4 = \frac{(0.71 \times e^{(0.28 \times SF)})}{(M_{ih}^{0.23})}$$

$$k_4 = \frac{(0.71 \times e^{(0.28 \times 3)})}{(13.9^{0.23})}$$

= 0.898

$f(P_{80}) = -(0.295 + 2200/1000000)$

= -0.297

$f(F_{80}) = -(0.295 + 30000/1000000)$

= -0.325

Hence:

$$W_{hc} = 13.9 \times 0.955 \times 1 \times 0.898 \times 4 \times (2200^{-0.297} - 30000^{-0.325})$$

$$= 3.17 \text{ kWh/t}$$

Step 5 - Estimate recycle load and machine throughput requirement:

For recycle load use Eq. (25):

$$\begin{aligned}
 \text{Recycle Load (\%)} &= \left(\frac{W_{hc}}{W_{hm}} - 1 \right) \times 100 \\
 &= \left(\frac{3.17}{1.11} - 1 \right) \times 100 \\
 &= 186\%
 \end{aligned} \tag{25}$$

Machine throughput requirement is estimated using Eq. (26):

$$\begin{aligned}
 \text{Machine throughput requirement (t/h)} &= \text{Circuitfreshfeedrate} \times \left(1 + \frac{\text{recycleload}}{100} \right) \\
 &= 1000 \times \left(1 + \frac{186}{100} \right) \\
 &= 2860 \text{ tph}
 \end{aligned} \tag{26}$$

Step 6 - Select a suitable HPGR:

The objective here is to select a roll diameter, length and speed which can process a throughput rate of 2860 tph plus a contingency to accommodate fluctuations in the circuit, provide “catch-up” capacity, give operational flexibility and account for uncertainty in the ore hardness of the deposit and the accuracy of the equations. Choosing appropriate machine dimensions and operating speed is an iterative process and is best done with the aid of a spreadsheet where experimenting with different combinations can be done rapidly. For the purposes of this worked example assume that a 25% contingency has been chosen, given that the design ore hardnesses are mean values. Hence the maximum throughput requirement of the selected HPGR is given by:

$$\begin{aligned}
 \text{Maximum machine throughput requirement (t/h)} &= 1.25 \times 2860 \\
 &= 3575 \text{ tph}
 \end{aligned}$$

Maximum machine throughput capacity of a HPGR is given by Eq. (6):

$$\text{Maximum throughput(t/h)} = 98 \times L \times D^{1.2} \times (0.68 \times D + 0.87) \times \rho_o \tag{6}$$

If we select a 2.5 m (diameter) \times 1.7 m (length) machine, then its expected maximum capacity using Eq. (6) is:

$$\begin{aligned}
 \text{Maximum throughput(t/h)} &= 98 \times 1.7 \times 2.5^{1.2} \times (0.68 \times 2.5 + 0.87) \times 2.8 \\
 &= 3600 \text{ tph}
 \end{aligned}$$

This is very similar to the maximum machine throughput requirement of 3575 tph so this machine can be selected.

A suitable motor size also has to be selected. Eq. (12) is used for this purpose:

$$\text{Installedpower(kW)} = 39 \times L \times D^{1.2} \times SF_{max} \times (0.68 \times D + 0.87) \times \rho_o \tag{12}$$

Most HPGR manufacturers design their full-scale machines to be capable of running with a maximum specific grinding force in the range 4–5 N/mm². Hence although we have assumed that the machine will be normally operated at 3 N/mm² it will be supplied with the capability of being operated with a maximum specific grinding force of 4–5 N/mm². Assume that in this case its maximum specific grinding force will be 4.5 N/mm². Eq. (12) estimates that to deliver this specific grinding force at maximum throughput capacity the installed power should be:

$$\begin{aligned}
 \text{Installed power(kW)} &= 39 \times 1.7 \times 2.5^{1.2} \times 4.5 \times (0.68 \times 2.5 + 0.87) \times 2.8 \\
 &= 6447 \text{ kW}
 \end{aligned}$$

This will be delivered by two motors (one for each roll), so each motor will be 3224 kW. Under normal operating conditions Eq. (17) has already estimated that the circuit net specific energy will be 3.17 kWh/t, which combined with a fresh feedrate of 1000 tph means that the net power draw of the HPGR in operation should be 3170 kW. Allowing 7.5% for drive losses indicates that the motor output power should be in total 3400 kW (1700 kW for each motor) - well inside the installed power.

Step 7 - Predict ball mill specific energy (W_{bm}):

In this step it is required to predict the ball mill specific energy to reduce in size the circuit feed (HPGR circuit product) 80% passing size of 2500 μ m to the ball mill cyclone overflow P80 of 150 μ m. This is done using equations 27, 28 and 29.

The specific energy to grind relatively coarse particles (W_a) is given by Eq. (27):

$$W_a = M_{ia} \times 4 \times (P_{80}^{f(P80)} - F_{80}^{f(F80)}) \tag{27}$$

In this case the P₈₀ is 750 μ m and the F₈₀ is 2500 μ m (HPGR circuit product). Hence:

$$\begin{aligned}
 f(P_{80}) &= -(0.295 + 750/1000000) \\
 &= -0.296 \\
 f(F_{80}) &= -(0.295 + 2200/1000000) \\
 &= -0.297 \\
 W_a &= 19.4 \times 4 \times (750^{-0.296} - 2200^{-0.297}) \\
 &= 3.07 \text{ kWh/t}
 \end{aligned}$$

The specific energy for grinding relatively fine particles (W_b) is given by Eq. (28):

$$W_b = M_{ib} \times 4 \times (P_{80}^{f(P80)} - F_{80}^{f(F80)}) \tag{28}$$

In this case the P₈₀ is 150 μ m and the F₈₀ is 750 μ m. Hence:

$$\begin{aligned}
 f(P_{80}) &= -(0.295 + 150/1000000) \\
 &= -0.295 \\
 f(F_{80}) &= -(0.295 + 750/1000000) \\
 &= -0.296 \\
 W_b &= 18.5 \times 4 \times (150^{-0.295} - 750^{-0.296}) \\
 &= 6.44 \text{ kWh/t}
 \end{aligned}$$

Having calculated W_a and W_b , Eq. (29) is used to determine the ball mill net specific energy. As there are no data available from testwork on our ore that indicates the extent to which HPGR treatment reduces ball mill feed hardness due to microcracking, the relationship in Fig. 13 is used. From this it is estimated that as the HPGR operating specific grinding force will be 3 N/mm^2 the microcracking allowance is about 5%, resulting in a K_{hpgr} value of 0.95. Hence:

$$\begin{aligned}
 W_{bm} &= K_{hpgr} \times (W_a + W_b) \\
 &= 0.95 \times (3.07 + 6.44) \\
 &= 9.03 \text{ kWh/t}
 \end{aligned} \tag{29}$$

Step 8 - Determine installed power:

As the design throughput rate is 1000 tph then the design net power draw is given by:

$$\begin{aligned}
 \text{Design net power draw (kW)} &= 1000 \times W_{bm} \\
 &= 1000 \times 9.03 \\
 &= 9030 \text{ kW}
 \end{aligned}$$

Given that the hardness values are mean values, assume a contingency of 25% and further assume that gearbox/drivetrain energy losses are 4%. On applying these allowances the required installed power (motor output power) is therefore given by:

$$\begin{aligned}
 \text{Required installed power (kW)} &= \frac{9030 \times 1.25}{0.96} \\
 &= 11764 \text{ kW}
 \end{aligned}$$

Step 9 - Select a ball mill that will draw the required installed power:

It has been decided to use an overflow discharge ball mill with a gear-and-pinion drive and a maximum ball load of 35% by volume.

Using Morrell's "C" model via SMC Testing's on-line tools (<https://www.smctestesting.com/tools/gross-power>), a $7.3 \text{ m} \times 11 \text{ m}$ (D \times L) mill with 20 deg cone ends, 125 mm liners, 35% balls, a discharge slurry density of 70% of solids by weight and running at 76% of critical speed will have a motor input power of 12100 kW. Assume that motor energy losses are 3% then the motor output power is given by:

$$\begin{aligned}
 \text{Motor output power (kW)} &= 12100 \times 0.97 \\
 &= 11737 \text{ kW}
 \end{aligned}$$

This is almost identical to the required installed power and hence this mill is selected. Depending on the equipment supplier chosen, the dimensions and installed motor size may vary slightly from those determined above so as to match standard sizes offered by the supplier. If the sizes do vary it is important to check that using the supplier's dimensions, speed and maximum ball load that the motor output power is predicted to be at least 11737 kW and that the suppliers recommended motor size is also at least 11737 kW.

Appendix C. Sizing and selecting a HPGR-HPGR circuit: Worked example

In this worked example the ball mill in the flowsheet option shown in Fig. 12 is replaced by an HPGR (see Fig. C1). It is a dry circuit and the hydrocyclone is replaced by an air classifier. As with the worked example in Appendix B the secondary crushing circuit, which feeds the primary HPGR circuit has already been designed and equipment selected to deliver crushed feed with an 80% passing size of 30 mm. The requirement of the primary HPGR circuit is to reduce this feed to an 80% passing size of 2.2 mm by operating the HPGR in closed circuit with a vibrating screen. This material is then fed to a secondary HPGR in closed circuit with an air classifier with a target fine stream P80 of 150 μm . The target circuit throughput rate is 1000 tph (see Table B3).

SMC Tests and Bond ball mill work index tests have been carried out on representative ore samples and the following results, which are the best estimates of the mean hardness values of the deposit, have been chosen as the basis for design:

Primary HPGR Circuit:

Step 1 - Choose an HPGR operating specific grinding force and determine the machine specific energy:

Most full-scale circuits operate in the specific grinding force (SF) range 2–4 N/mm^2 so choose 3 N/mm^2 . Using Eq. (9):

$$W_{hm} (\text{kWh/t}) = 0.37 \times SF \tag{9}$$

Hence:

$$\begin{aligned}
 W_{hm} &= 0.37 \times 3 \\
 &= 1.11 \text{ kWh/t}
 \end{aligned}$$

Step 2 - Predict the HPGR circuit specific energy (W_{hc}) to reduce the circuit feed with an F_{80} of 30000 μm to a circuit product with a P_{80} of 2200 μm . This is done using Eq. (17):

$$W_{hc} = M_{ih} \times S_h \times k_3 \times k_4 \times 4 \times (P_{80}^{f(P80)} - F_{80}^{f(F80)}) \tag{17}$$

Where:

W_{hc} = predicted net specific energy of the HPGR circuit (kWh/t)

M_{ih} = SMC Test® HPGR hardness parameter (kWh/t)

$$= 13.9 \text{ kWh/t}$$

S_h = coarse feed factor

$$= 35 \times (F_{80} \times P_{80})^{-0.2} : (0.5 < S_h < 1)$$

$$= 35 \times (30000 \times 2200)^{-0.2}$$

$$= 0.955$$

$$= 1.0 \text{ for closed circuit}$$

$$k_4 = \frac{(0.71 \times e^{(0.28 \times SF)})}{(M_{ih}^{0.23})}$$

$$k_4 = \frac{(0.71 \times e^{(0.28 \times 3)})}{(13.9^{0.23})}$$

$$= 0.898$$

$$f(P_{80}) = -(0.295 + 2200/1000000)$$

$$= -0.297$$

$$f(F_{80}) = -(0.295 + 30000/1000000)$$

$$= -0.325$$

Hence:

$$W_{hc} = 13.9 \times 0.955 \times 1 \times 0.898 \times 4 \times (2200^{-0.297} - 30000^{-0.325})$$

$$= 3.17 \text{ kWh/t}$$

Step 3 - Estimate recycle load and machine throughput requirement:

For recycle load use Eq. (25):

$$\begin{aligned} \text{Recycle Load (\%)} &= \left(\frac{W_{hc}}{W_{hm}} - 1 \right) \times 100 \\ &= \left(\frac{3.17}{1.11} - 1 \right) \times 100 \\ &= 186\% \end{aligned} \quad (25)$$

Machine throughput requirement is estimated using Eq. (26):

$$\begin{aligned} \text{Machine throughput requirement (t/h)} &= \text{Circuit fresh feed rate} \times \left(1 + \frac{\text{recycle load}}{100} \right) \\ &= 1000 \times \left(1 + \frac{186}{100} \right) \\ &= 2860 \text{ tph} \end{aligned} \quad (26)$$

Step 4 - Select a suitable HPGR:

The objective here is to select a roll diameter, length and speed which can process a throughput rate of 2860 tph plus a contingency to accommodate fluctuations in the circuit, provide “catch-up” capacity, give operational flexibility and account for uncertainty in the ore hardness of the deposit and the accuracy of the equations. Choosing appropriate machine dimensions and operating speed is an iterative process and is best done with the aid of a spreadsheet where experimenting with different combinations can be done rapidly. For the purposes of this worked example assume that a 25% contingency has been chosen, given that the design ore hardnesses are mean values. Hence the maximum throughput requirement of the selected HPGR is given by:

$$\begin{aligned} \text{Maximum machine throughput requirement (t/h)} &= 1.25 \times 2860 \\ &= 3575 \text{ tph} \end{aligned}$$

Maximum machine throughput capacity of a HPGR is given by Eq. (6):

$$\text{Maximum throughput (t/h)} = 98 \times L \times D^{1.2} \times (0.68 \times D + 0.87) \times \rho_o \quad (6)$$

If we select a 2.5 m (diameter) \times 1.7 m (length) machine, then its expected maximum capacity using Eq. (6) is:

$$\begin{aligned} \text{Maximum throughput (t/h)} &= 98 \times 1.7 \times 2.5^{1.2} \times (0.68 \times 2.5 + 0.87) \times 2.8 \\ &= 3600 \text{ tph} \end{aligned}$$

This is very similar to the maximum machine throughput requirement of 3575 tph so this machine can be selected.

A suitable motor size also has to be selected. Eq. (12) is used for this purpose:

$$\text{Installed power (kW)} = 39 \times L \times D^{1.2} \times SF_{max} \times (0.68 \times D + 0.87) \times \rho_o \quad (12)$$

Most HPGR manufacturers design their full-scale machines to be capable of running with a maximum specific grinding force in the range 4–5 N/mm². Hence although we have assumed that the machine will be normally operated at 3 N/mm² it will be supplied with the capability of being operated with a maximum specific grinding force of 4–5 N/mm². Assume that in this case its maximum specific grinding force will be 4.5 N/mm². Eq. (12) estimates that to deliver this specific grinding force at maximum throughput capacity the installed power should be:

$$\begin{aligned} \text{Installed power (kW)} &= 39 \times 1.7 \times 2.5^{1.2} \times 4.5 \times (0.68 \times 2.5 + 0.87) \times 2.8 \\ &= 6447 \text{ kW} \end{aligned}$$

This will be delivered by two motors (one for each roll), so each motor will be 3224 kW. Under normal operating conditions Eq. (17) has already estimated that the circuit net specific energy will be 3.17 kWh/t, which combined with a fresh feedrate of 1000 tph means that the net power draw of the HPGR in operation should be 3170 kW. Allowing 7.5% for drive losses indicates that the motor output power should be in total 3400 kW (1700 kW for each motor) - well inside the installed power.

Secondary HPGR Circuit:

Step 5 - Choose an HPGR operating specific grinding force and determine the machine specific energy:

Most full-scale circuits operate in the specific grinding force (SF) range 2–4 N/mm² so choose 3 N/mm². Using Eq. (9):

$$W_{hm}(\text{kWh/t}) = 0.37 \times SF \quad (9)$$

Hence:

$$\begin{aligned} W_{hm} &= 0.37 \times 3 \\ &= 1.11 \text{ kWh/t} \end{aligned}$$

Step 6: Predict the HPGR circuit specific energy (W_{hc}) to reduce the circuit feed with an F_{80} of 2200 μm to a circuit product with a P_{80} of 150 μm . This is done using Eq. (17):

$$W_{hc} = M_{ih} \times S_h \times k_3 \times k_4 \times 4 \times (P_{80}^{f(P_{80})} - F_{80}^{f(F_{80})}) \quad (17)$$

Where:

W_{hc} = predicted net specific energy of the HPGR circuit (kWh/t)

M_{ih} = SMC Test® HPGR hardness parameter (kWh/t)

$$= 13.9 \text{ kWh/t}$$

S_h = coarse feed factor

$$= 35 \times (F_{80} \times P_{80})^{-0.2} : (0.5 < S_h < 1)$$

$$= 35 \times (2200 \times 150)^{-0.2}$$

$$= 2.76$$

As $0.5 < S_h < 1$ then in this case:

$$S_h = 1$$

K_3 = open/closed circuit factor

$$= 1.0 \text{ for closed circuit}$$

$$k_4 = \frac{(0.71 \times e^{(0.28 \times SF)})}{(M_{ih}^{0.23})}$$

$$k_4 = \frac{(0.71 \times e^{(0.28 \times 3)})}{(13.9^{0.23})}$$

$$= 0.898$$

$$f(P_{80}) = -(0.295 + 150/1000000)$$

$$= -0.295$$

$$f(F_{80}) = -(0.295 + 2200/1000000)$$

$$= -0.297$$

Hence:

$$\begin{aligned} W_{hc} &= 13.9 \times 1 \times 1 \times 0.898 \times 4 \times (150^{-0.295} - 2200^{-0.297}) \\ &= 6.31 \text{ kWh/t} \end{aligned}$$

Step 7: Estimate recycle load and machine throughput requirement.

For recycle load use Eq. (25):

$$\begin{aligned} \text{Recycle Load (\%)} &= \left(\frac{W_{hc}}{W_{hm}} - 1 \right) \times 100 \\ &= \left(\frac{6.31}{1.11} - 1 \right) \times 100 \\ &= 468\% \end{aligned} \quad (25)$$

Machine throughput requirement is estimated using Eq. (26):

$$\begin{aligned} \text{Machine throughput requirement (t/h)} &= \text{Circuit fresh feedrate} \times \left(1 + \frac{\text{recycle load}}{100} \right) \\ &= 1000 \times \left(1 + \frac{468}{100} \right) \\ &= 5680 \text{ tph} \end{aligned} \quad (26)$$

Step 8: Select a suitable HPGR.

The objective here is to select a roll diameter, length and speed which can process a throughput rate of 5680 tph plus a contingency to accom-

moderate fluctuations in the circuit, provide “catch-up” capacity, give operational flexibility and account for uncertainty in the ore hardness of the deposit and the accuracy of the equations. Choosing appropriate machine dimensions and operating speed is an iterative process and is best done with the aid of a spreadsheet where experimenting with different combinations can be done rapidly. For the purposes of this worked example assume that a 25% contingency has been chosen, given that the design ore hardnesses are mean values. Hence the maximum throughput requirement of the selected HPGR is given by:

$$\begin{aligned} \text{Maximum machine throughput requirement } (t/h) &= 1.25 \times 5680 \\ &= 7100 \text{ tph} \end{aligned}$$

Maximum machine throughput capacity of a HPGR is given by Eq. (6):

$$\text{Maximum throughput } (t/h) = 98 \times L \times D^{1.2} \times (0.68 \times D + 0.87) \times \rho_o \quad (6)$$

The largest HPGR currently available is a 3 m × 2 m unit which, according to Eq. (6) should give a maximum throughput capacity of about 6000 tph. This is not sufficient to meet the throughput requirement of 7100 tph. However, the primary HPGR which is a 2.5 m × 1.7 m unit has a maximum throughput capacity of 3600 tph and hence two of these in parallel will be able to meet the 7100 tph requirement. Therefore, these HPGRs are also selected for secondary duty. This has the added advantage in that the required spares inventory can be minimised, which saves costs.

The motor size is also the same as the primary HPGR but as there are two machines the total installed capacity is $2 \times 6447 = 12894$ kW. As the predicted circuit net specific energy is 6.31 kWh/t then with a target circuit throughput of 1000 tph the expected net power draw in operation should be 6310 kW or 6783 kW motor output – well inside the total installed power.

References

- Andersen, J. S. 1988., Development of a Cone Crusher Model, M.Eng.Sc thesis, JKMR, University of Queensland, Australia.
- AngloAmerican, 2021. Climate Change Report 2021. <https://www.angloamerican.com/~media/Files/A/Anglo-American-Group/PLC/sustainability/approach-and-policies/environment/climate-change-report-2021.pdf>.
- Antofagasta, 2020. Climate Change. <https://www.antofagasta.co.uk/media/4132/climate-change.pdf>.
- Aydoğan, N.A., Ergün, L., Benzer, H., 2006. High pressure grinding rolls (HPGR) applications in the cement industry. *Minerals Engineering* 19 (2), 130–139.
- Ballantyne, G.R., Di Trento, M., Lovatt, I. and Putland, B., 2017. Recent Improvements in the Milling Circuit at Tropicana Mine. *Proc. Metplant 2017*, Perth, Australia.
- Banini, G.A., 2002. An integrated description of rock breakage in comminution machines. University of Queensland, Australia. Ph.D thesis, JKMR.
- Barrick Corp, 2021. Barrick Updates its Evolving Emissions Reduction Target. https://s25.q4cdn.com/322814910/files/doc_news/2021/04/Barrick-Updates-its-Evolving-Emissions-Reduction-Target.pdf.
- BHP, 2021. Climate transition Action Plan. https://www.bhp.com/~media/document/s/investors/annual-reports/2021/210914_bhpclimatetransitionactionplan2021.pdf?sc_lang=en&hash=EB11097F5500602D2928F09D4EF081DB.
- Bond, F.C., 1959. Confirmation of the Third Theory. AIME Annual Meeting, San Francisco, California, USA.
- Bond, F.C., 1961a. Crushing and Grinding Calculations Part 1. *Brit. Chem Eng.* 6 (6), 378–385.
- Bond, F.C., 1961b. Crushing and Grinding Calculations Part 2. *Brit. Chem Eng.* 6 (6), 543–548.
- Buckingham, L., Dupont, J-F., Steiger, J., Blain, B. and Brits, C., 2011. Improving Energy Efficiency in Barrick Grinding Circuits. *Proc. SAG 2011*, Vancouver, Canada.
- Burns, N., Gauld, C., Alvim, M. D. and Tagami, M., 2019. Technical Report – Salobo III Expansion. https://s21.q4cdn.com/266470217/files/doc_downloads/2020/03/Salobo-Technical-Report-FINAL.pdf.
- CIM Magazine, 2018, <https://magazine.cim.org/en/technology/on-a-roll-en-1/>.
- CITIC, 2021. <https://www.citic-hic.com/data/upload/2015-11/20151110072914949494.pdf>.
- Comi, T., Burchardt, E., 2015. A Premier for Chile: The HPGR Based Copper Concentrator of Sierra Gorda SCM. In: *Proc. SAG 2015*, Vancouver, Canada.
- Daniel, M.J., 2007. Energy efficient mineral liberation using HPGR technology, PhD thesis, JKMR, School of Engineering, University of Queensland, Australia.
- Daniel, M., Lane, G., McLean, E., 2010. Efficiency, economics, energy and emissions-emerging criteria for comminution circuit decision making. In: *Proc. XXV IMPC*, Brisbane, Queensland, Australia.
- Demus, T., Echterhof, T., Pfeifer, H. and Quicker, P., 2012. Investigations on the Use of Biogenic Residues as Substitutes for Fossil Coal in the EAF Steelmaking Process. In: *Proc. 10th European Electric Steelmaking Conference*, Graz, Austria.
- Dindorf, R., Wos, P., 2020. Energy-Saving Hot Open Die Forging Process of Heavy Steel Forgings on an Industrial Hydraulic Forging Press. *Energies* 13 (7), 17.
- Dowling, E.C., Korpi, P.A., McIvor, R.E., Rose, D.J., 2001. Application of High Pressure grinding Rolls in an Autogenous-Pebble Milling Circuit. *Proc. SAG 2001*, Vancouver, Canada.
- EIA, 2020. How much carbon dioxide is produced per kilowatt hour of U.S. electricity generation? <https://www.eia.gov/tools/faqs/faq.php?id=74&t=11>.
- Engelhardt, D., Seppelt, J., Waters, T., Apfelt, A., Lane, G., Yahyaie, M., and Powell, M., 2015. The Cadia HPGR-SAG Circuit – From Design to Operation – The Commissioning Challenge. *Proc. SAG 2015*, Vancouver, Canada.
- Fortescue, 2021. https://www.fmgl.com.au/docs/default-source/announcements/target-to-achieve-net-zero-scope-3-emissions.pdf?sfvrsn=195d0b1f_4.
- Fortescue, 2019. Iron Bridge Project Approval. https://www.fmgl.com.au/docs/default-source/announcements/iron-bridge-project-approval.pdf?sfvrsn=8cdff6a3_4.
- Freeport-McMoran, 2020. Climate Report <https://www.fcx.com/sites/fcx/files/documents/sustainability/2020-Climate-Report.pdf>.
- Giblett, A., Seidel, J., 2011. Measuring, Predicting and Managing Grinding Media Wear. *Proc. SAG 2011*, Vancouver, Canada.
- Glencore, 2020. Climate Report 2020: Pathway to Net Zero. <https://www.glencore.com/media-and-insights/news/Climate-Report-2020-Pathway-to-Net-Zero>.
- GMG Group, 2016. Morrell Method for Determining Comminution Circuit Specific Energy and Assessing Energy Utilization Efficiency of Existing Circuits <https://gmgroup.org/guidelines/>.
- Griffith, A.A., 1921. The Phenomena of Rupture and Flow in Solids. *Philos. Trans. R. Soc. London. Series A* 221.
- Hart S., Parker B., Rees T., Manesh A., & McGaffin I. 2011. Commissioning and Ramp Up of the HPGR Circuit at Newmont Boddington Gold, *Proc. SAG 2011*, Vancouver, Canada.
- KHD, 2012. https://www.khd.com/tl_files/downloads/products/grinding-technology/grinding/roller-presses-cement/KHD_ROLLER_PRESS_April_2012.pdf.
- Koepfer, 2021. https://www.koepfer-international.com/fileadmin/_migrated/content_uploads/Koepfer_High-Pressure_Grinding_01.pdf.
- Koski, S., Vanderbeek, J.L., Enriquez, J., 2011. Cerro Verde Concentrator – Four Years Operating HPGRs. *Proc. SAG 2011*, Vancouver, Canada.
- Klymowsky, R. 2003. High Pressure Grinding Rolls for Minerals. https://www.ausimm.com/globalassets/insights-and-resources/minerals-processing-toolbox/polysius_hpg_r.pdf.
- Kock, F., Siddall, L., Lovatt, I., Giddy, M. and Di Trento, M. 2015. Rapid Ramp-Up of the Tropicana Circuit. In: *Proc. SAG 2015*, Vancouver, Canada.
- Lane, G., Foggatto, B., Bueno, M., 2013. Power-based comminution calculations using Ausgrind. *Proc. Procemin 2013*, Santiago, Chile.
- Lathiredi, S., Morrell, S., 2003. Slurry flow in mills: grate-pulp lifter discharge systems (Part 2). *Minerals Eng.* 16(7), 635–642.
- Macivor, R.E.E., Dowling, E.C., Korpi, P.A., and Rose, D.J. 2001. Application of high pressure grinding rolls in an autogenous-pebble milling circuit. *Proceedings SAG 2001*, Vancouver, Canada.
- Metso, 2021. <https://www.mogroup.com/portfolio/hrc-series/hrce/>.
- Mining Technology, 2021. Iron Bridge Magnetite Project. <https://www.mining-technology.com/projects/iron-bridge-magnetite-project/>.
- Morley, C., 2010. HPGR – FAQs. *SAIMM*, vol 110, pp 107-115.
- Morrell, S., 1996. Power draw of wet tumbling mills and its relationship to charge dynamics—Part 1: A continuum approach to mathematical modelling of mill power draw. *Trans. Inst. Min. Metall. Section C* 105, C43–C53.
- Morrell, S., 2003. Grinding mills: how to accurately predict their power draw. In: *Proceedings XXII International Mineral Processing Congress*, Cape Town, South Africa, SAIMM, pp 50-59.
- Morrell, S., 2004a. Predicting the specific energy of autogenous and semi-autogenous mills from small diameter drill core samples. *Miner. Eng.* 17 (3), 447–451.
- Morrell, S., 2004b. An alternative energy-size relationship to that proposed by bond for the design and optimisation of grinding circuits. *Int. J. Miner. Process.* 74, 133–141.
- Morrell, S., 2008. A method for predicting the specific energy requirement of comminution circuits and assessing their energy utilisation efficiency. *Minerals Eng.* 21 (3), 224–233. <https://doi.org/10.1016/j.mineng.2007.10.001>.
- Morrell, S., 2009. Predicting the overall specific energy requirement of crushing, high pressure grinding roll and tumbling mill circuits. *Miner. Eng.* 22 (6), 544–549.
- Morrell, S. 2011. The Appropriateness of the Transfer Size in AG and SAG Mill Circuit Design. In: *Proc. SAG 2011*, Vancouver, Canada.
- Mular, M.A., Hoffer, J.R., and Koski, S. M., 2015. Design and Operation of the Metcalf Concentrator. *Proc. SAG 2015*, Vancouver, Canada.
- Newmont, 2020. Climate Strategy Report. https://s24.q4cdn.com/382246808/files/doc_downloads/sustainability/2020-report/Newmont-Climate-Strategy-Report.pdf.
- Otte, O., 1988. *Polycom High Pressure Grinding Principles and Industrial Application*. In: Cobar, N.S.W. (Ed.), *Third Mill Operators' Conference*. Australia, pp. 131–135.

- Palmer, E., Dixon, S., Meadows, D., 2011. An Update of the SAG Milling Operation at the Penasquito Mine Located in the Zactecas State, Mexico. Proc. SAG 2011, Vancouver, Canada.
- Parker, B., Rowe, P., Lane, G., Morrell, S., 2001. The decision to opt for high pressure grinding rolls for the Boddington expansion. SAG 2001, Vancouver, Canada, pp. 93–106.
- Patzelt, N., Knecht, J., Burchardt, E., Klymowsky, R., 2000. Challenges for High Pressure Grinding in the New Millennium. In: Kalgoorlie, W.A. (Ed.), Seventh Mill Operators Conference. Australia, pp. 47–55.
- Pehl, P., Arvesen, A., Humpenoder, F., Popp, A., Hertwich, E.G., Luderer, G., 2017. Understanding future emissions from low-carbon power systems by integration of life cycle assessment and integrated energy modelling. *Nature Energy* 2, 939–945.
- Polysius, 2021. https://ucpcdn.thyssenkrupp.com/_legacy/UCPhyssenkruppBAIS/assets/files/products_services/mineral_processing/grinding_plants/polycom_en.pdf.
- Rashidi, S., Rajamani, R.K., Fuerstenau, D.W., 2017. A Review of the Modelling of High Pressure Grinding Rolls. *KONA Powder Particle J.* 34, 125–140.
- Rio Tinto, 2021. Our Approach to Climate Change 2020. <https://www.riotinto.com/-/media/Content/Documents/Invest/Reports/Climate-Change-reports/RT-climate-report-2020.pdf?rev=c415a8138bd7408496ccb3834511abc0>.
- Rule, C.M., Fouchee, R.J., Swart, W.C.E., 2015. HPGR Operation at Mogalakwena Concentrators. Proc. SAG 2015, Vancouver, Canada.
- Saramak, D., Kleiv, R.A., 2013. The effect of feed moisture on the comminution efficiency of HPGR circuits. *Minerals Eng.* 43–44, 105–111.
- Stephenson, I., 1997. The downstream effects of high pressure grinding rolls processing. PhD Thesis. JKMR, University of Queensland, Australia.
- Scinto, P., Festa, A., Putland, B., 2015. OMC Power-based comminution calculations for design, modelling and circuit optimization. In: Proc. 47th Annual Meeting CMP. Ottawa, Canada.
- Tavares, L.M., King, R.P., 1998. Single-particle fracture under impact loading. *Int. J. Miner. Process.* 54, 1–28.
- Tozlu, F.J., Fresko, M., 2015. Autogenous and Semi-Autogenous Mills 2015 Update. In: Proc SAG 2015, Vancouver, Canada.
- Vale, 2021. Climate Change Report 2021. http://www.vale.com/esg/pt/Documents/Vale_CC_2021-EN.pdf.
- Van Der Meer, F.P., 1997. HPGR Grinding of Pellet Feed. Experiences of KHD in the Iron Ore Industry. In: AusIMM Conference on Iron Ore Resources and Reserves Estimation. 25–26 September 1997, Perth, WA, Australia.
- Van der Meer, F.P., 2015. Pellet Feed Grinding by HPGR. *Minerals Eng.* 73, 21–30.
- Van der Meer, F.P., Maphosa, W., 2012. High pressure grinding moving ahead in copper, iron, and gold processing. *SAIMM* 112, 637–647.
- Vanderbeek J.L., Linde T.B., Brack W.S., Marsden J.O. 2006. HPGR Implementation at Cerro Verde, Proc. SAG 2006, Vancouver, Canada.
- Villanueva, A., Banini, G., Hollow, J., Butar-Butar, R., Mosher, J., 2011. Effects of HPGR Introduction on Grinding Performance at PT Freeport Indonesia's Concentrator. Proc. SAG 2011. Vancouver, Canada.
- Wong, H., Mackert, T., Lipiec, T., Remmers, J., Burchardt, E., Vanderbeek, J.L., 2019. Optimising Ball Mill Selection for a HPGR Ball Mill Circuit. Proc. SAG 2019, Vancouver, Canada.
- Wong, H., 2020. Private communication, 22nd September 2020.
- World Energy Data, 2021, World Electricity Generation 2020 <https://www.worldenergydata.org/world-electricity-generation/>.
- World Steel Association. 2017. Steel's Contribution to a Low Carbon Future. <https://www.steel.org.au/resources/elibrary/resource-items/steel-s-contribution-to-a-low-carbon-future-and-cl/download-pdf.pdf/#:~:text=The%20greenhouse%20gas%20of%20most,of%20total%20world%20CO2%20emissions>.
- Zervas, G. 2019. The Metcalf Concentrator HRC™3000: Performance at Variable Specific Force. Proc. SAG 2019, Vancouver, Canada.